POLITECNICO DI TORINO

Master's Degree in Mechatronic Engineering

Master's Degree Thesis

Direct Virtual Sensor design for radar localization systems

Supervisors

Prof. NOVARA CARLO

Prof. MILANESE MARIO

Candidate

FRANCESCO NATALE

Academic Year 2022/2023

Summary

In recent decades, a large amount of studies have been focusing on target tracking using radar measurements. Radar systems typically measure the position of the target in polar coordinates, but in many applications it is of interest to obtain the target Cartesian coordinates. However, due to measurement noise, the conversion from polar to Cartesian coordinates using the classical trigonometric formulas may lead to inaccurate results. This problem can be mitigated by using an observer/filter, which can attenuate the noise effects and provide a more accurate estimate of the target Cartesian coordinates. Designing a state observer, the main two following phases have to be expected: first identifying a system model from an experimental data set, and then designing an observer based on the identified model. This two-step approach might be problematic due to some nonlinearities in the identified model. So, a one-step approach is preferable, since the data set is used to direct design the filter and not for identification of the model. The aim of this thesis is to design both the two-step and the one-step procedures in order to highlight the differences between the two and to put an accent to the solution that gets better performances, based on simulations. Regarding the first method, an Extended Kalman Filter (EKF) has been designed in Simulink, while in the one-step procedure a Direct Virtual Sensor (DVS) is engineered using Simulink, the System Identification Toolbox and neural networks. Through the simulations, the results got in terms of root-mean-square error, do give evidence that the proposed one-step procedure may be better than the two-faces described above.

Acknowledgements

I am extremely grateful to my supervisors, Prof. Carlo Novara and Prof. Mario Milanese for their invaluable advice, constant support, and their patience during the development of this thesis. I am also thankful to Modelway SRL for all the support.

"Gutta Cavat Lapidem"
Ovidius

Contents

List of Tables

List of Figures

Acronyms

2D

2 dimensions

3D

3 dimensions

ARMAX

Auto-Regressive Moving Average with eXogenous Inputs

ARX

Auto-Regressive with eXogenous Input

CRLB

Cramèr-Rao Lower Bound

DVS

Direct Virtual Sensor

EKF

Extended Kalman Filter

EM

Electromagnetic

IFF

Identification Friend or Foe

KF

Kalman Filter

LIDAR

Laser Imaging Detection and Ranging

LQR

Linear-Quadratic Regulator

LTI

Linear Time-Invariant

ML

Maximum Likelihood Estimator

MTI

Moving Target Indication

MV

Minimum Variance Estimator

NARMAX

Nonlinear Auto-Regressive Moving Average with eXogenous Inputs

NARX

Nonlinear Auto-Regressive Moving Average with eXogenous Inputs

NOE

Nonlinear Output Error

OE

Output Error

pdf

Probability density function

PF

Particle Filter

RCS

Radar Cross Section

RF

Radio-frequency, Radar Frequency

RMS

Root-mean-square

RMSE

Root-mean-square error

rpm

Revolution per minute

SISO

Single-Input and Single-Output

SNR

Signal to Noise Ratio

UKF

Unscented Kalman Filter

Chapter 1

Introduction

Target tracking estimation is employed in many application areas. The estimation of position and velocity is performed by a huge number of radar applications such as inertial navigation systems, surveillance systems, remote sensing and environmental monitoring systems, global positioning systems, differential positioning systems, air traffic control, and satellite orbit determination. Using emitted electromagnetic radiation and analyzing the echo coming from reflecting objects, the targets, a radar operates. Knowledge about the target may be gleaned from the echo signal's characteristics. The duration needed for the radiation to reach the target and back provides the range or distance from the target. A directional antenna (e.g. with limited bandwidth) is used to identify the arrival angle of the echo signal to determine its angular location. A radar can determine the target's track, or trajectory, and can estimate its future location if it is moving. Although a stationary echo signal could be several orders of magnitude larger than the moving target, a radar can differentiate between desired moving targets (like aircraft) and unwanted stationary targets (like land and sea clutter) because of the shift in frequency of the obtained echo signal caused by the Doppler effect induced by a moving target. A radar can determine details about the size and shape of the target, given a sufficiently high resolution. Unlike a large amount of optical and infrared sensors, a radar is an active instrument that includes its transmitter, and it does not rely on environmental radiation. The main benefit of the radar over other sensors is its ability to accurately state a target's range throughout all weather conditions and regardless its distance from reference. Range, angle, or both may be employed to evaluate the accuracy of the radar: large bandwidth is recommended for range resolution and angle resolution involves employing large antennas. A huge chuck of radar application development is supported by military and defense applications. Nevertheless, radar has found large use also in civil applications, including safe navigation of ships, planes and spacecraft, environmental remote sensing, self-driving vehicles, and weather monitoring. Due to the exponential growth of this radar applications usage, the technical improvements have been challenging plenty of engineers during the last years [1][2]. As previously stated, the measurements of a target position in a radar system are addressed in polar coordinates (its range and azimuth), but the target dynamics are modeled in Cartesian coordinates. The transformation from spherical coordinates to Cartesian ones may generate bias in measurements error. To figure out this problem, a tracking filter may be designed. A large number of filters are used in literature. The Extended Kalman Filter (EKF), which is the expansion of the Kalman Filter (KF), is used to deal with nonlinear functions. The EKF deals with Taylor series expansion to linearize nonlinear states or/and measurement equations. The EKF is unable to claim the KF's optimal solution for the linear-Gaussian system, because of the approximation. However, the EKF is the most used filter because it is easy to set up and simple to use in many samples, including radar and sonar tracking applications. The Unscented Kalman Filter (UKF) estimates the variable's distribution using a sampling technique that gathers a set of samples nearly the mean of the estimation variables. The aligned distributions are faithfully depicted by any nonlinear transformations, such as the measurements and state dynamics. The mean measurement covariance and state estimates are instantaneously propagated. Just a minimal number of predetermined particles known as sigma points are employed by the UKF to establish initial densities. Unlike the EKF, those points may compute the mean and covariance of the nonlinearity at least second order, and the Jacobian matrix computation is not required. Although if the UKF has a more refined approach and is derivative-free regards to the EKF, it has two main downside. Firstly, the nonlinearity could be so severe that predicting mean and covariance might need even higher order accuracy than the UKF can offer. The second problem is that even though the first two instants may be precisely computed, the densities might be significantly non-Gaussian, allowing them inadequate. The Particle Filter (PF) or Sequential Monte Carlo (SMC) explains problems of nonlinearity and the problem of localization if there are no sciences about the position of the target. To depict densities, the PF propagates an ensemble of particles. The Monte Carlo method runs and these particles are chosen randomly. The number of particles required to depict the pdf is greater than the sigma point of UKF. Furthermore, the PF is simpler to implement than the EKF, but its main problem is the computational difficulty. The PF is available in an large number of varieties, such as the Regularized Particle Filter (RPF), Markov Chain Monte Carlo step Particle Filter (MCMC-PF), classical Sequential Importance Resampling (SIR), and Auxiliary Sequential Importance Resampling (ASIR) particle filter [3][4][5][6][7][8]. In the case of knowledge of differentiable equations of the system to be studied and the observability of the variable to estimate, a **state observer/filter** might be designed. But, in real-world application, the system to be filtered is not known. However, a set of experimental data is known a priori, so a standard approach is to first identify the model from that data set and then design a filter from identified model. This procedure, known as **two-step approach**, has multiple faults: the identified model is only approximated, and a filter that is optimal for the identified model could have a large estimation error when applied to the real system. Dealing with a nonlinear system, only an approximate filter can be derived, which stability is not yet guaranteed [9]. To avoid this inconvenience a new filter design may be adopted, through a **one-step approach**. The filter is directly designed from the experimental data set, without identifying first the model structure. This direct approach allows to skip problems coming from the model estimation. The Kalman Filter's performance degradation owing to modeling errors may be substantially greater, hence it can not guarantee a comparable result. An example of this Direct Filtering (DF) is the **Direct Virtual Sensor** (DVS), which is good for designing also nonlinear systems. Hence, the direct approach marks a paradigm leap in filter design, allowing to develop of the best filter even for nonlinear systems, while resolving crucial issues like model uncertainty and nonlinear filter approximation [6][9][10].

In this thesis, both a two-step approach and a one-step approach are considered. In the first approach, an EKF is designed using Simulink, using the main block after defining useful functions and parameters, while in the second one, a DVS is implemented using the System Identification Toolbox in MATLAB and neural networks (a default number of sigmoid functions). Differences between the two main approaches are defined in terms of root-mean-square error, and the validations are performed for both the positions $\mathbf{x}$ and $\mathbf{y}$ and both the velocities $\mathbf{v_x}$ and $\mathbf{v_y}$. Simulation results show that in **DVS** case the RMSE values are better for every reference taken into account than the **EKF** obtained values.

In chapter 2 the two-step approach and the use of the EKF are presented, in chapter 3 a theoretical view of the two different approaches is presented, in both cases of LTI and nonlinear system, in chapter 4 some radar theory and examples are submitted, in chapter 5 the two-step and one-step procedure are well explained, in particular the design of DVS is accounted, in chapter 6 the simulations results and the performances of the proposed tracking filters are presented, in chapter 7 conclusions are summarized.

Chapter 2

Two-step approach: using the Extended Kalman Filter

The Kalman filter algorithm estimates unknown variables from a set of data that is collected over time and corrupted by noise. The KF is largely used in the orbit calculation field, target tracking and navigation, tracking of maneuvering targets, and positioning of GPS. The KF is a linear optimal status estimation method. Since the Kalman filter is pertinent only for linear systems, when dealing with nonlinear systems the most used observer is the Extended Kalman Filter. The core concept of the EKF is to obtain a linear equation from a nonlinear system, by focusing on the value of a first-order nonlinear Taylor expansion around the estimated status. Taylor expansion is a linear process, hence the EKF outcomes are widely close to the true value, if the system status and observation equations are linear and continuous. Note that the filtering result is corrupted by the status and measurement noise [11]. Consider the discrete-time nonlinear system [12]:

$$\mathbf{x}_{k+1} = f(\mathbf{x}_k, \mathbf{u}_k) + \mathbf{d}_k \tag{2.1}$$
$$\mathbf{y}_k = h(\mathbf{x}_k) + \mathbf{d}_k^y \tag{2.2}$$

where:

- $k \in \mathbb{Z}$ is the discrete time;
- $\mathbf{x}_k$ is the state;
- $\mathbf{u}_k$ is the input;
- $\mathbf{y}_k$ is the output;
- $\mathbf{d}_k$ is a disturbance;

- $\mathbf{d}_k^y$ is a measurement noise.

Dealing with a linear system, it is possible to enunciate:

$$f(\mathbf{x}_k, \mathbf{u}_k) = \mathbf{F}_k \mathbf{x}_k + \mathbf{G}_k \mathbf{u}_k \tag{2.3}$$
$$h(\mathbf{x}_k) = \mathbf{H}_k \mathbf{x}_k \tag{2.4}$$

where $\mathbf{y}_k, \mathbf{u}_k$ are measurable. A huge number of state observers work to compute a prediction $\mathbf{x}_k^p$ of the state $\mathbf{x}_k$, using:

$$\mathbf{x}_k^p = f(\hat{\mathbf{x}}_{k-1}, \mathbf{u}_{k-1}), \tag{2.5}$$

then adjust the prediction using the current output measurement:

$$\hat{\mathbf{x}}_k = \mathbf{x}_k^p + \mathbf{K}_k \boldsymbol{\Delta} \mathbf{y}_k \tag{2.6}$$

where:

$$\boldsymbol{\Delta} \mathbf{y}_k = \mathbf{y}_k - h(\mathbf{x}_k^p). \tag{2.7}$$

Regarding linear systems (Equation 2.3 and Equation 2.4) the gain matrix $\mathbf{K}_k$ is chosen to lessen the variance of the estimation error norm ($\mathbf{E}[\|\mathbf{x}_k - \hat{\mathbf{x}}_k\|_2^2]$). If the system is nonlinear, it is linearized along the trajectory to get the matrices, so $\mathbf{F}_k$ and $\mathbf{H}_k$ are the Jacobian matrices:

$$\mathbf{F}_k := \mathbf{J}_f(\mathbf{x}_k, \mathbf{u}_k) = \begin{bmatrix} \frac{\delta f_1}{\delta x_1} & \dots & \frac{\delta f_1}{\delta x_{n_x}} & \frac{\delta f_1}{\delta u_1} & \dots & \frac{\delta f_1}{\delta x_{n_u}} \\ \dots & \dots & \dots & \dots & \dots & \dots \\ \frac{\delta f_{n_x}}{\delta x_1} & \dots & \frac{\delta f_{n_x}}{\delta x_{n_x}} & \frac{\delta f_{n_x}}{\delta u_1} & \dots & \frac{\delta f_{n_x}}{\delta x_{n_u}} \end{bmatrix} (\mathbf{x}_k, \mathbf{u}_k) \in \mathbb{R}^{n_x, n_x + nu} \tag{2.8}$$

$$\mathbf{H}_k := \mathbf{J}_h(\mathbf{x}_k) = \begin{bmatrix} \frac{\delta h_1}{\delta x_1} & \dots & \frac{\delta h_1}{\delta h_{n_x}} \\ \dots & \dots & \dots \\ \frac{\delta h_{n_y}}{\delta x_1} & \dots & \frac{\delta f_{n_y}}{\delta x_{n_x}} \end{bmatrix} (\mathbf{x}_k) \in \mathbb{R}^{n_y, n_x} \tag{2.9}$$

The following quantities are so defined:

- $\hat{\mathbf{x}}_k$ is the estimate of $\mathbf{x}_k$, computed at step k;
- $\hat{\mathbf{x}}_k^p$ is the prediction of $\mathbf{x}_k$, computed at step $k-1$;
- $\mathbf{P}_k \doteq \mathbf{E}[(\mathbf{x}_k - \hat{\mathbf{x}}_k)(\mathbf{x}_k - \hat{\mathbf{x}}_k)^T]$ is the covariance matrix of $\mathbf{x}_k - \hat{\mathbf{x}}_k$;
- $\mathbf{Q}^d \doteq \mathbf{E}[(\mathbf{d}_k \mathbf{d}_k^T)]$ is the covariance matrix of $\mathbf{d}_k$;
- $\mathbf{R}^d \doteq \mathbf{E}[(\mathbf{d}_k^y (\mathbf{d}_k^y)^T)]$ is the covariance matrix of $\mathbf{d}_k^y$;

Firstly, $\mathbf{Q}^d$ and $\mathbf{R}^d$ must be initialized as diagonal matrices, with $\mathbf{d}_k$ and $\mathbf{d}_k^y$ on the diagonal. Note that a trial and error procedure may be required if poor information are given from the $\mathbf{d}_k$ and $\mathbf{d}_k^y$. Then, the estimated initial state $\hat{\mathbf{x}}_0$ (typically $\mathbf{0}$) and the estimated initial covariance matrix $\mathbf{P}_0$ (typically $\mathbf{I}$) are initialized. The EKF algorithm may be summarized in the two following steps:

Prediction:

$$\mathbf{x}_k^p = f(\mathbf{x}_{k-1}, \mathbf{u}_{k-1}) \tag{2.10}$$

$$\mathbf{P}_k = \mathbf{F}_{k-1}\mathbf{P}_{k-1}\mathbf{F}_{k-1}^T + \mathbf{Q}^d \tag{2.11}$$

Update:

$$\mathbf{S}_k = \mathbf{H}_k\mathbf{P}_k^p\mathbf{H}_k^T + \mathbf{R}^d \tag{2.12}$$

$$\mathbf{K}_k = \mathbf{P}_k^p\mathbf{H}_k^T\mathbf{S}_k^{-1} \tag{2.13}$$

$$\mathbf{\Delta y}_k = \mathbf{y}_k - h(\mathbf{x}_k^p) \tag{2.14}$$

$$\hat{\mathbf{x}}_k = \mathbf{x}_k^p + \mathbf{K}_k\mathbf{\Delta y}_k \tag{2.15}$$

$$\mathbf{P}_k = (\mathbf{I} - \mathbf{K}_k\mathbf{H}_k)\mathbf{P}_k^p \tag{2.16}$$

In the prediction step, a preliminary estimate of the state is obtained from the model equations. Lastly, in the update step, the preliminary estimate is corrected according to the current output measurement.

Chapter 3

Filter design from data: two-step vs. one-step

Considering a discrete-time system S, [9] described by the following state equations:

$$\mathbf{x}^{t+1} = \mathbf{F}(\mathbf{x}^t, \tilde{\mathbf{u}}^t) + \mathbf{w}_x^t \tag{3.1}$$
$$\tilde{\mathbf{y}}^t = \mathbf{H}_y(\mathbf{x}^t, \tilde{\mathbf{u}}^t) + \mathbf{w}_y^t \tag{3.2}$$
$$\tilde{\mathbf{z}}^t = \mathbf{H}_z(\mathbf{x}^t, \tilde{\mathbf{u}}^t) + \mathbf{w}_z^t \tag{3.3}$$

where:

- $\mathbf{x}^t \in X \subseteq \mathbb{R}^{n_x}$ is the state;
- $\tilde{\mathbf{u}}^t \in U \subseteq \mathbb{R}^{n_u}$ is the known input;
- $\tilde{\mathbf{y}}^t \in Y \subseteq \mathbb{R}^{n_y}$ is the measured output;
- $\tilde{\mathbf{z}}^t \in Y \subseteq \mathbb{R}^{n_z}$ is the variable to estimate;
- $\mathbf{w}_x^t$ is the process noise;
- $\mathbf{w}_y^t$ and $\mathbf{w}_z^t$ are the output noise.

The aim is designing a filter that, knowing the inputs $\tilde{\mathbf{u}}^t$ and $\tilde{\mathbf{y}}^t$, $\tau \leq t$, gives an estimate of $\tilde{\mathbf{z}}^t$. The filter is denoted as DVS. Notice that the direct approach, despite of the two-step procedure, allows to design finest filters, without uncertainty model problems and nonlinear filter approximation. Assuming as basic assumptions: $(\mathbf{F}, \mathbf{H}_y)$ observable, the functions $\mathbf{F}, \mathbf{H}_y$ and $\mathbf{H}_z$ in Equation 3.1, Equation 3.2, and Equation 3.3 not known, an available set of data $\{\tilde{\mathbf{u}}^t, \tilde{\mathbf{y}}^t, \tilde{\mathbf{z}}^t, t = 1{,}2, \ldots, T\}$, the $\mathbf{w}_x^t$,

$\mathbf{w}_y^t$ and $\mathbf{w}_z^t$ as stochastic variables, and $\bar{\mathbf{E}}\mathbf{v}^t \doteq \lim_{T\to\infty} \frac{1}{T}\sum_{t=1}^{T} \mathbf{E}\mathbf{v}^t$, knowing that $\mathbf{E}$ is the mean value.
The two-step procedure involves to identify the mathematical model from data set, and design the filter from the model. In the first step, the model is stated as:

$$\mathbf{M}(\boldsymbol{\theta}_M) : \boldsymbol{\theta}_M \in \boldsymbol{\Theta}_M \tag{3.4}$$

where $\boldsymbol{\Theta}_M$ is a subset of $\mathbb{R}^{n_{\theta M}}$ and $n_{\theta M}$ is the number of parameters of the model structure. The model structure outlines the model set:

$$\mathcal{M} \doteq \{\mathbf{M}(\boldsymbol{\theta}_M) : \boldsymbol{\theta}_M \in \boldsymbol{\Theta}_M\} \tag{3.5}$$

From the above data set, a model $\hat{\mathbf{M}}$ is identified:

$$\mathbf{D}_M \doteq \{\tilde{\mathbf{u}}^t, (\tilde{\mathbf{y}}^t, \tilde{\mathbf{z}}^t), t = 1,2,\ldots,T\} \tag{3.6}$$

In Equation 3.6 $\tilde{\mathbf{u}}^t$ is the input of the model, while $(\tilde{\mathbf{y}}^t, \tilde{\mathbf{z}}^t)$ are the output. Then a filter $\hat{\mathbf{K}} \equiv \mathbf{K}(\hat{\boldsymbol{\theta}}_M)$ is designed to estimate $\tilde{\mathbf{z}}^t$. The filter $\hat{\mathbf{K}}$ gives an output which is an estimate $\hat{\mathbf{z}}_K^t$ of $\tilde{\mathbf{z}}^t$. A relevant note is that, in the two-step approach the filter structure can not be chosen, but it depends on the identified model.
In direct approach, the filter is identified from data set, not from the mathematical model. In this second procedure a structure is selected:

$$\mathbf{V}(\boldsymbol{\theta}_V) : \boldsymbol{\theta}_V \in \boldsymbol{\Theta}_V \tag{3.7}$$

where $\boldsymbol{\Theta}_V$ is a subset of $\mathbb{R}^{n_{\theta V}}$ and $n_{\theta V}$ is the number of parameters of the filter structure. The filter set defined from the filter structure is:

$$\mathcal{V} \doteq \{\mathbf{V}(\boldsymbol{\theta}_V) : \boldsymbol{\theta}_V \in \boldsymbol{\Theta}_V\} \tag{3.8}$$

So, a filter $\hat{\mathbf{V}}$ is identified from the following data set:

$$\mathbf{D}_V \doteq \{\tilde{\mathbf{u}}^t, (\tilde{\mathbf{y}}^t, \tilde{\mathbf{z}}^t), t = 1,2,\ldots,T\} \tag{3.9}$$

Even if both the sets $\mathbf{D}_M$ and $\mathbf{D}_V$ use the same data, they are different each other. With the respect to the two-step approach, where the filter $\hat{\mathbf{K}}$ can not be chosen, in one-step procedure, the filter $\hat{\mathbf{V}}$ can be chosen. This filter is the **Direct Virtual Sensor (DVS)**. In following sections differences between one-step and two-step approaches are explained in linear and nonlinear cases.

3.0.1 Linear system

The case of linear system S is examined. Given a linear model $\mathbf{M}(\boldsymbol{\theta}_M)$ of order n_M, the equivalent KF $\mathbf{K}(\boldsymbol{\theta}_M)$ is linear, stable of order n_M. Hence, if $\mathbf{V}(\boldsymbol{\theta}_M)$ is a filter of order n_M, then $\mathbf{K}(\boldsymbol{\theta}_M) \in \mathcal{V}$. The following theorem is presented if the assumptions in Section 3.1 in [9] are verified.

Theorem 1

Noted probability equal to 1 as $T \to \infty$, the obtained results are:

1. $\hat{\mathbf{V}} = \arg\min_{V(\theta_V)} \bar{\mathbf{E}}\|\tilde{\mathbf{z}}^t - \hat{\mathbf{z}}_V^t\|^2$.
2. If $\hat{\mathbf{K}} \in \mathcal{V}$, then $\bar{\mathbf{E}}\|\tilde{\mathbf{z}}^t - \hat{\mathbf{z}}_V^t\|^2 \leq \bar{\mathbf{E}}\|\tilde{\mathbf{z}}^t - \hat{\mathbf{z}}_K^t\|^2$.
3. If $\mathbf{S} = \mathbf{M}(\boldsymbol{\theta}_M^0) \in \mathcal{M}$ and $\mathbf{K}(\boldsymbol{\theta}_M^0) \in \mathcal{V}$, then $\hat{\mathbf{V}}$ is a minimum variance filter among all linear casual filter mapping $(\tilde{\mathbf{u}}^t, \tilde{\mathbf{y}}^t) \to \tilde{\mathbf{z}}^t, \tau \leq t$.
4. If $\mathbf{S} = \mathbf{M}(\boldsymbol{\theta}_M^0) \in \mathcal{M}$ and $\mathbf{K}(\boldsymbol{\theta}_M^0) \in \mathcal{V}$, $\mathbf{M}(\boldsymbol{\theta}_M)$ is globally identifiable, $\mathbf{S}$ is stable, and the data are informative enough, then $\bar{\mathbf{E}}\|\tilde{\mathbf{z}}^t - \hat{\mathbf{z}}_V^t\|^2 = \bar{\mathbf{E}}\|\tilde{\mathbf{z}}^t - \hat{\mathbf{z}}_K^t\|^2$.

When the system S is stable, the filter $\hat{\mathbf{K}}$, under the assumption that the model structure fit perfectly the system, is asymptotically optimal. While dealing with an unstable system S, the filter $\hat{\mathbf{V}}$ is resulting better than $\hat{\mathbf{K}}$.

3.0.2 Nonlinear system

The case of nonlinear system S is examined [9]. A filter structure $\mathbf{V}(\boldsymbol{\theta}_V)$ is taken into account, which satisfy condition M1 (see Appendix of [9]) and it is related to the following regression equation:

$$\hat{\mathbf{z}}_V^t = f_V(\boldsymbol{\theta}_V, \hat{\mathbf{z}}_V^{t-1}, \ldots, \hat{\mathbf{z}}_V^{t-n_V}, \tilde{\mathbf{y}}^t, \ldots, \tilde{\mathbf{y}}^{t-n_V}, \tilde{\mathbf{u}}^t, \ldots, \tilde{\mathbf{u}}^{t-n_V}) \tag{3.10}$$

Note that, also the minimum variance filter $\hat{\mathbf{K}}$ can be described by the regression equation:

$$\hat{\mathbf{z}}_K^t = f_V(\hat{\boldsymbol{\theta}}_V, \hat{\mathbf{z}}_V^{t-1}, \ldots, \hat{\mathbf{z}}_V^{t-n_V}, \tilde{\mathbf{y}}^t, \ldots, \tilde{\mathbf{y}}^{t-n_V}, \tilde{\mathbf{u}}^t, \ldots, \tilde{\mathbf{u}}^{t-n_V}) \tag{3.11}$$

After verifying the assumption in [9] in Section 3.2, the following theorem can be stated:

Theorem 2

Noted probability equal to 1 as $T \to \infty$, the obtained results are:

1. $\hat{\mathbf{V}} = \arg\min_{V(\theta_V)} \bar{\mathbf{E}}\|\tilde{\mathbf{z}}^t - \hat{\mathbf{z}}_V^t\|^2$.
2. If $\hat{\mathbf{K}} \in \mathcal{V}$, then $\bar{\mathbf{E}}\|\tilde{\mathbf{z}}^t - \hat{\mathbf{z}}_V^t\|^2 \leq \bar{\mathbf{E}}\|\tilde{\mathbf{z}}^t - \hat{\mathbf{z}}_K^t\|^2$.
3. If $\mathbf{S} = \mathbf{M}(\boldsymbol{\theta}_M^0) \in \mathcal{M}$ and $\mathbf{K}(\boldsymbol{\theta}_M^{\mathbf{0}}) \in \mathcal{V}$, then $\hat{\mathbf{V}}$ is a minimum variance filter.

After studying the *Theorem 2*, the advantages of one-step procedure compared to the two-step in linear case, are extended also in the case of nonlinear systems. In this last case, the minimum variance filter $\hat{\mathbf{K}}$ can not be computed, but only approximations of that. Thence, the improvement of direct approach is more evident for nonlinear system with respect to the linear case.

3.1 DVS design procedure

Knowing the following set of data $\mathbf{D}_V \doteq \{\tilde{\mathbf{u}}^t, (\tilde{\mathbf{y}}^t, \tilde{\mathbf{z}}^t), t = 1,2,\ldots,T\}$, if the set of Equations 3.1, 3.2, 3.3 are linear, a linear filter could be stated (e.g. ARX, OE, ARMAX), while if the cited equations are nonlinear, a nonlinear one could be designed (e.g. NARX, NOE, NARMAX) and the function f_V in Equation 3.10 has to be chosen taking into account some parameterizations (e.g. neural networks, polynomials functions, etc.). The design of DVS is different depending on the linearity or nonlinearity of the system S. If S is linear, the DVS has design:

$$\hat{\mathbf{z}}_V^t = \hat{\boldsymbol{\theta}}_V \cdot (\hat{\mathbf{z}}_V^{t-1}, \ldots, \hat{\mathbf{z}}_V^{t-n_V}, \tilde{\mathbf{y}}^t, \ldots, \tilde{\mathbf{y}}^{t-n_V}, \tilde{\mathbf{u}}^t, \ldots, \tilde{\mathbf{u}}^{t-n_V}) \tag{3.12}$$

While, if the system S is nonlinear, the designed DVS is stated as:

$$\hat{\mathbf{z}}_V^t = f_V(\hat{\boldsymbol{\theta}}_V, \hat{\mathbf{z}}_V^{t-1}, \ldots, \hat{\mathbf{z}}_V^{t-n_V}, \tilde{\mathbf{y}}^t, \ldots, \tilde{\mathbf{y}}^{t-n_V}, \tilde{\mathbf{u}}^t, \ldots, \tilde{\mathbf{u}}^{t-n_V}) \tag{3.13}$$

Note that, in both Equations 3.12 and 3.13 the $\hat{\boldsymbol{\theta}}_\mathbf{V} \in \mathbb{R}^{n_z \times n_V(n_z+n_y+n_u)}$.

Chapter 4

Principles of radar

4.1 Measurements of a radar

A **radar** is an electrical device that emits radiofrequency (RF) electromagnetic (EM) waves in the direction of a target area, then get and recognizes the EM waves which are reflected from detecting objects [13]. The main subsystem requires a **transmitter**, an **antenna**, a **receiver**, and a **signal processor**: the transmitter allows to generate the EM waves, the antenna, as a subsystem, receives as input these EM waves from the transmitter and places them into the propagation medium (e.g. the atmosphere). The antenna and the transmitter are connected each other via a transmit/receive device (T/R device). The T/R device provides a connection point, enabling simultaneous attachment of both the transmitter and the receiver to the antenna, and it includes also isolation between the two, to preserve receiver components from the high-powered transmit signal. In the target domain, the transmitted signal is propagated, and in the target itself currents are induced by the EM waves, so it re-radiates these currents in the surrounding area. The signal may be re-radiated also by other surfaces on the ground, these unwanted signals are called **clutter**. The radar antenna "captures" the piece of the signal that is reflected from the object which propagates back to the radar antenna, applying it to the receiver circuits. Receiver's components amplify the received signal, transform the RF signal into an intermediate frequency (IF), apply the signal to an analog-to-digital (ADC), and finally apply the signal to the signal/data processor.
Discussing the received target signal, the presence of the interference must be a case of study. The interference may occur in different forms:

- Internal and external electronic noise;
- Reflected EM waves from undesired objects, called clutter;

- Unwanted external EM waves sorted by human-made source, like the electromagnetic interference (EMI);
- Intentional jamming from an electronic countermeasures (ECM) system.

Estimating the presence of a target, and dealing with noise, clutter, and jamming is one of the main task of the radar's signal processor [13].

4.1.1 Fundamental of radar measurements

The electromagnetic energy emitted by a radar allows the target's echo to be used to analyze and receive information about the target. The localization of a target is obtained after collecting information about it, and it is developed in 3 dimensions or 2 dimensions. To localize the target position, accurate measurements are required: distance and angle (azimuth and elevation) with respect to the reference point. Estimate a Radar Cross Section (RCS) and radial velocity of the target is a desirable plus. Moreover, using the observed range, transmitted and received pulse powers, and a propagation model (radar range equation), a radar calculated the RCS. Polar (spherical) coordinates are obtained due to the estimation of azimuth and elevation angular direction. Several parameters may be obtained:

- **Range** ($\mathbf{R}$), which is estimated by calculating the two-way time delay of the transmitted signal;
- **Range rate** ($\dot{\mathbf{R}}$) or **radial velocity**, which is calculated by determining the Doppler shift of the echo signal;
- **Angular position**, which is determined by comparing the signal strength of several antenna beams offset in angle from another one and obtained either with an antenna design that constitutes multiple offset beams (like mono-pulse), or by examining a single beam across or close to the target.

The target tracking process involves repeatedly taking the radar range, angle, and radial velocity measurements, combining them through kinematic state estimation, or filtering the measurements to produce more accurate two-dimensional position and velocity or three-dimensional position, velocity, and acceleration estimates. Track filtering algorithms are the results of combining those individual measurements [13].

4.1.2 Model for radar signal

To provide radar measurements, voltage signals are often used. As a result, modeling and analysis of the measurements for tracking studies, require the voltage form of the radar signal. A general model of the RF echo signal which is received by the radar, in both cases of a conventional antenna or the sum channel of a mono-pulse coming from a single target, may be stated due to the proportionality of the voltage and the square root of power, so:

$$\mathbf{s}(t) = \mathbf{2}\sqrt{\frac{\mathbf{P}_t}{(\mathbf{4}\boldsymbol{\pi})^3}}\frac{\boldsymbol{\lambda}}{\mathbf{R}^2}\boldsymbol{\xi}\mathbf{V}_s^2(\boldsymbol{\theta},\boldsymbol{\phi})\mathbf{p}(t)\,\mathbf{cos}(\boldsymbol{\omega}_c t + \boldsymbol{\omega}_d t + \boldsymbol{\psi}) + \mathbf{w}_s(t) \tag{4.1}$$

where:

- $\mathbf{P}_t$ is the transmitted power;
- $\boldsymbol{\lambda}$ is the wavelength;
- $\mathbf{R}$ is the range to the target;
- $\boldsymbol{\xi}$ is the voltage reflectivity of the target;
- $\mathbf{V}_s(\boldsymbol{\theta},\boldsymbol{\phi})$ is the voltage gain of the antenna at the angles $(\boldsymbol{\theta},\boldsymbol{\phi})$;
- $(\boldsymbol{\theta},\boldsymbol{\phi})$ is the angular location of the target relative to antenna boresight;
- $\mathbf{p}(t)$ is the envelope of the matched filter output for the transmitted pulse;
- $\boldsymbol{\omega}_c$ is the carrier frequency of the transmitted waveform;
- $\boldsymbol{\omega}_d$ is the Doppler shift of the received waveform;
- $\boldsymbol{\psi}$ is the phase of the target echo;
- $\mathbf{w}_s(t)$ is the receiver noise.

The voltage reflectivity $\boldsymbol{\xi}$ of the target is related to $\boldsymbol{\sigma}$ (RCS):

$$\boldsymbol{\sigma} = \frac{\boldsymbol{\xi}^2}{\mathbf{2}} \tag{4.2}$$

Due to the square of the term $\mathbf{V}_s(\boldsymbol{\theta},\boldsymbol{\phi})$ in Equation 4.1, it is stated a priori that the normalized antenna voltage gain model is the same in transmission and reception. The $\mathbf{V}_s(\boldsymbol{\theta},\boldsymbol{\phi})$ is assumed to be:

$$\mathbf{V}_s(\boldsymbol{\theta},\boldsymbol{\phi}) = \mathbf{W}(\boldsymbol{\theta})\mathbf{U}(\boldsymbol{\phi}) \tag{4.3}$$

where $\mathbf{W}(\boldsymbol{\theta})$ and $\mathbf{U}(\boldsymbol{\phi})$ are the elevation and azimuth voltage patterns.
The measured amplitude of the signal $\mathbf{s}(t)$ may be reduced due to two main faults [13]:

1. If $\mathbf{s}(t)$ is combined with $\boldsymbol{\omega}_c$ instead of $\boldsymbol{\omega}_c + \boldsymbol{\omega}_d$, in the related filter a frequency mismatch arises, generating a Doppler loss (a loss in SNR). If a radar is originally designed for air targets and it used for detect and track while traveling space targets when velocity is high, the Doppler loss could have a significant value to prevent detection;

2. The output of the matched filter must be sampled regularly in fast time at the bandwidth of the signal throughout the range interval (range window) of interest, due to the necessity to identify targets at a priori unknown ranges and to detect multiply and close together objects in the same dwell. One of the samples may or may not fall on the peak of the matching filter response. Besides that, the target echo's energy may be absorbed in closed samples that cross the peak, reducing the respective SNR (this reduction is often noted as straddle loss). Moreover, the signal in the neighboring cells may increase range estimate precision beyond resolution and decrease straddle loss.

4.1.3 Estimation of parameters

Estimation of the different target characteristics reflected in the signal is the purpose of the radar measurement process in the signal $\mathbf{s}(t)$. Before explanations on the measurements and estimation of the parameters including reflectivity amplitude, $\boldsymbol{\xi}$, the Doppler shift, $\boldsymbol{\omega}_d$, the angular direction to the target, $(\boldsymbol{\theta}, \boldsymbol{\phi})$, and the time delay to the target, it is necessary to discuss the **estimator** and his precision [13].

Estimators

A sum of the target component $\mathbf{s}(t)$ and noise component $\mathbf{w}(t)$ deals in the **observed signal** $\mathbf{y}(t)$:

$$\mathbf{y}(t) = \mathbf{s}(t) + \mathbf{w}(t) \tag{4.4}$$

The $\mathbf{y}(t)$ is a function of one or more parameters $(\boldsymbol{\alpha}_i)$ (i.e. time delay, amplitude, Doppler shift, or angle of arrival (AOA) of the target component). An estimator is designed to estimate the parameter values if a set of observations of $\mathbf{y}(t)$ is known. A vector of N observations is obtained considering a sampled multiple timed the signal $\mathbf{y}(t)$:

$$\mathbf{Y} = \{\mathbf{y}_1, \mathbf{y}_2, \ldots, \mathbf{y}_N\} \tag{4.5}$$

The data $\mathbf{Y}$ is a random vector that depends on the parameter $\boldsymbol{\alpha}$, and a conditional pdf $\mathbf{p}(\mathbf{Y}|\boldsymbol{\alpha})$ relates the $\mathbf{Y}$. An estimator f of a parameter $\boldsymbol{\alpha}$, based on a $\mathbf{Y}$ data is:

$$\hat{\boldsymbol{\alpha}} = f(\mathbf{Y}) \tag{4.6}$$

The estimator is unbiased and consistent, so the estimate's variance drops to zero when additional measurements are available, and the estimate's expected value is equal to the parameter's actual value:

$$\mathbf{E}\{\hat{\boldsymbol{\alpha}}\} = \boldsymbol{\alpha}_i \tag{4.7}$$

$$\lim_{N\to\infty} \{\boldsymbol{\sigma}^2_{\hat{\alpha}}\} \to \mathbf{0} \tag{4.8}$$

So, an optimal estimator has accurate estimates and his precision enhances dealing with more data.
In literature, a large amount of estimators exist. The most used are **minimum variance** (**MV**) estimators and **maximum likelihood** (**ML**) estimators. The minimum variance, or **minimum variance unbiased** (**MVU**) estimator is unbiased and it reduces the mean square error between the estimated value of the parameter and the actual value. The **maximum likelihood** (**ML**) estimator chooses $\hat{\boldsymbol{\alpha}}$ to maximize the likelihood of the observed data values $\mathbf{Y}$. Since it is rather simple to identify its form, the ML estimator is often an excellent practical choice. Moreover, it is comparable to the MV estimator in the case of Gaussian noise, so it is the ideal estimator. As was already discussed, the measurement precision is described by the standard deviation of the estimation error. Starting from the chosen estimator, the standard deviation is so derived, but it can be difficult to calculate for a certain estimator.

4.1.4 Range measurements

After explaining the outcomes of resolution and sampling, in the following subsections additional methods and accuracy analysis are discussed. Range and angle measurements are the main topics of the resolution and sampling discussion, but these tasks also concern phase and Doppler measurements [13].

Resolution and Sampling

Typically, a radar gathers target returns all over a limited time delay or range window for each pulse that is transmitted. The resolution of the range may be expressed as:

$$\Delta\mathbf{R} = \boldsymbol{\alpha}\frac{\mathbf{c}}{\mathbf{2B}} \tag{4.9}$$

where $\mathbf{B}$ is the waveform bandwidth, $\boldsymbol{\alpha}$ stands as the degradation in range resolution from system errors or range side lobe reduction techniques (e.g. windowing), and $\mathbf{1} < \boldsymbol{\alpha} < \mathbf{2}$. The $\mathbf{B}/\boldsymbol{\alpha}$ is bandwidth of the intermediate frequency (IF) filters and it defines the Nyquist sampling rate when the output of matched filter occurs. Precisely location of a closely spaced targets and the differentiation between them is bounded depends on the resolution of the radar system. A radar angular and range resolution may be depicted as a system whence a 3 dB beamwidth coming from the system and it is bounded by two ideal black lines. It is denoted by $\boldsymbol{\theta}_\mathbf{3}$

and it is subdivided into some range bins, named **range gates**. As an example, in these range bins may occur some targets. A sample of the output of the filter which is matched to is associated with each range bin, is used to pass the received echo signal through. If the output of the matched filter overtakes the detection threshold, an estimation of the range and angle is obtained. As an example three types of situations may be described, considering as target an airplane: (1) the airplane is smaller than the range cell, but it stands along two range cells, so the echoed energy from the aircraft is split between two adjacent range cells causing straddle loss, (2) two closed airplanes stand in the same range cell, so only one measurement with energy from both target outcomes, (3) the larger airplane stands over three range cells, so significant echoes from the airplane are observed in three consecutive matched filter's samples, these targets are often called extended targets. In radar tracking, deciding whether sequence of detection is one extended target or multiple closely spaced targets is a portion of the challenge.

4.1.5 Phase measurement

If the Doppler shift is known, the signal phase may be estimated. If the frequency in known, the Equation 4.1 may be stated as:

$$\mathbf{s}(t) = \mathbf{p}(t)\,\mathbf{cos}(\boldsymbol{\omega} t + \boldsymbol{\phi}) \tag{4.10}$$

where $\boldsymbol{\omega}$ is the frequency, and $\boldsymbol{\phi}$ is the carrier phase. About the phase, in literature, is demonstrated that the best estimator is:

$$\hat{\boldsymbol{\phi}} = -\,\mathbf{tan}^{-1}\frac{\mathbf{P}_s}{\mathbf{P}_c} \tag{4.11}$$

$$\mathbf{P}_s = \int \mathbf{p}(t)\,\mathbf{sin}(\boldsymbol{\omega} t)\;dt \tag{4.12}$$

$$\mathbf{P}_c = \int \mathbf{p}(t)\,\mathbf{cos}(\boldsymbol{\omega} t)\;dt \tag{4.13}$$

If the SNR is large enough, the RMS error is:

$$\boldsymbol{\sigma}^2_{\hat{\phi}} \geq \frac{\mathbf{1}}{\mathbf{SNR}\cdot\boldsymbol{\tau}\mathbf{B}} \tag{4.14}$$

where $\boldsymbol{\tau}\mathbf{B}$ is the pulse time-bandwidth product [13].

4.1.6 Doppler and range rate measurements

Usually, pulsed Doppler waveforms which include a periodic sequence of pulses, are used to achieve range rate measurements. During the processing, using the whole range window for each pulse for time delay esteem, the matched filter output is sampled. The estimation of the Doppler frequency $\mathbf{f}_d$, and the related radial velocity $\mathbf{v} = \mathbf{2f}_d/\boldsymbol{\lambda}$, is performed through a discrete Fourier transform processing the samples of the matched filter output coming from the multiple pulses at each range. The range rate, $\dot{R}$, is the negative of the radial velocity. The inverse of the duration of the pulse-Doppler waveform dwell time T_d is the inverse of the peak-to-null (Rayleigh) Doppler resolution:

$$\boldsymbol{\Delta}\mathbf{f}_d = \frac{\mathbf{1}}{\mathbf{T}_d} \tag{4.15}$$

Since $\mathbf{f}_d = \mathbf{2v}/\boldsymbol{\lambda}$, the velocity resolution and the range rate resolution are:

$$\boldsymbol{\Delta}\mathbf{v} = \boldsymbol{\Delta}\dot{\mathbf{R}} = \frac{\boldsymbol{\lambda}}{\mathbf{2T}_d} = \frac{\mathbf{c}}{\mathbf{2T}_d\mathbf{f}_t} \tag{4.16}$$

where $\mathbf{f}_t$ is the carrier frequency of the transmitted waveform. Potential ambiguities in range and range rate may occur in a pulse-Doppler waveform. So, the minimum range (not considering ambiguities) is:

$$\mathbf{R}_{ua} = \frac{\mathbf{cT}}{\mathbf{2}} \tag{4.17}$$

where $\mathbf{T}$ is the slow-time sampling interval (PRI). The interval which causes ambiguity in Doppler frequency is $\mathbf{1/T}$ Hz. The maximum unambiguous Doppler frequency, velocity, and range rate, if interested frequencies are both positive and negative, are given by:

$$\mathbf{f}_{d_{ua}} = \pm\frac{\mathbf{1}}{\mathbf{2T}} = \pm\frac{\mathbf{PRF}}{\mathbf{2}} \tag{4.18}$$

$$\mathbf{v}_{ua} = \dot{\mathbf{R}}_{ua} = \pm\frac{\boldsymbol{\lambda}}{\mathbf{2}}\mathbf{PRF} = \pm\frac{\mathbf{c}}{\mathbf{2f}_t}\mathbf{PRF} \tag{4.19}$$

Where PRF is the pulse repetition frequency [13].

4.1.7 Angle measurements

The angular location of the target is not obtained when an EM echo is received from a standard antenna system, in this case only information about the possible localization in the main lobe of the beam are gathered. Once a target has a high RCS, it may not stand in the 3 dB beamwidth of the antenna pattern. The amplitudes of the echoed signals are acquired for multiple positions of the antenna boresight as it scans by the target in a huge number of radars that rotate to scan the field of vision, and centroiding is used to determine the angular location of the target. Since many beam positions are required to overcome the RCS fluctuations of the target while reaching an accurate angle-of-arrival estimate, centroiding the signal for multiple positions of the antenna pattern is not an optimal solution; this fault refers to tracking radars that support control functions, radars which measure two angular coordinates and electronically scanned radars which scan while tracking. One of the early strategy employed to improve the angle measurements of these radars is the so-called **sequential lobing**, which involves two consecutive steps to enhance each angular measurement. After identifying the target, the antenna's boresight is facing slightly to one side of the target's predicted location while estimating the first measurement, then the boresight is facing to the other side of the predicted position while estimating the second measurement. Thanks to this procedure a better evaluate the predicted angle of the target is obtained. Note that this sequential lobing is useful since it is sensitive to pulse-to-pulse amplitude fluctuations of target echos, a common behavior of radar measurements [13].

4.1.8 Coordinate system

The target location is determined by a radar system using spherical coordinates relatively the boresight of a radar antenna:

- Range, **R**;
- Azimuth angle, $\boldsymbol{\theta}$;
- Elevation angle, $\boldsymbol{\phi}$.

The azimuth angle and elevation angle are measured in orthogonal planes when a coordinate system is centered on the antenna. The following layout is initially stated: the x direction is the "horizontal" dimension of the antenna, the z direction is the "vertical" dimension of the antenna, and the y dimension is the normal in relation to the antenna face. The azimuth angle is measured in the horizontal x-y plane, while the elevation angle is measured from the horizontal x-y plane in the vertical plane. Typically, operating in a Cartesian coordinate system is preferable than using the spherical coordinates. So, a Cartesian system (x-y-z) can be centered on the radar platform or to any reference point. In Equation 4.20, Equation 4.21, and Equation 4.22, the transformation from the angle computation to the antenna-centered Cartesian coordinates is shown:

$$x = R\cos\theta\cos\phi \tag{4.20}$$

$$y = R\sin\theta\cos\phi \tag{4.21}$$

$$z = R\sin\theta \tag{4.22}$$

An important notice is the representation of the coordinates in 3-dimensions. Starting from the spherical coordinate errors, a nonlinear combination of them explains the measurement errors in Cartesian coordinates. These errors are coupled: the error in x, the error in y, and the error in z are dependent each other. So, the conversion in polar coordinates is explicated as [13]:

$$R = \sqrt{x^2 + y^2 + z^2} \tag{4.23}$$

$$\theta = \tan^{-1} \frac{y}{x} \tag{4.24}$$

$$\phi = \cos^{-1} \frac{z}{R} \tag{4.25}$$

4.2 Frequencies of radars

The radar frequencies have no inherent limits. A radar is any device that detects and locates a target by emitting electromagnetic radiation and using the reflected echo from the target, no matter what frequency it operates. Radars is applied to deal both with a few megahertz and with the ultraviolet region of the spectrum. The fundamental principles are the same, no matter the frequency, but the actual implementation is different. Each frequency range has unique characteristics which make it more suitable for some applications than others. The different electromagnetic spectrum bands are explained below. Note that the distinctions between the frequency areas are not so stringent in real-world applications [2].

HF (from 3 to 30 MHz). A number of disadvantages deal whit radar applications using this frequency band. Huge antennas are needed to accomplish narrow beamwidths, the level of the natural ambient noise is high, the accessible bandwidths are limited, and this region of the electromagnetic spectrum is heavily used and constrained. Additionally, because of the long wavelength, a large number of potential targets may be in the Rayleigh region, where the target's dimensions are small compared to the wavelength; as a result, the radar cross section of the target is small with respect to the (HF) wavelength and it may be lower than the cross section when microwave frequencies are considered. According to the ionosphere's current condition, HF electromagnetic waves have the crucial quality of being refracted by it, going back to the Earth at distance between 500 and 2000 nmi (Nautical Mile). The aircraft over the horizon may be detected due to this property. The HF region of the spectrum is interesting for the radar monitoring of regions (such as oceans) where it is difficult to use conventional microwave radar due to the large over-the-horizon ranges which are achievable.

VHF (from 30 to 300 MHz). Similar to the HF region, the VHF (Very High Frequency) region is overflowed, bandwidths are reduced, external noise may be high, and beamwidths are large. An enhancement in the maximum range against some aircraft may deal when constructive interference occurs between direct wave and reflected wave, with horizontal polarization over a good reflecting surface. Since the range is rising due to the constructive interference, the coverage of other elevation angles is aborted by the coupled destructive interference, and the energy at low angles is reduced. This frequency range is useful for lower-cost radars and long-range radars. Furthermore, since the drawbacks are more evident than the advantages, this radar type is no longer used.

UHF (from 300 to 1000 MHz). This frequency band has the same properties as the previous one, but the natural external noise has fewer drawbacks and the beamwidths are tinier than the ones of VHF. If the antenna is large, dealing with a reliable long-range surveillance radar it is a good frequency area. It is good for AEW (Airborne Early Warning), e.g. airborne radar which uses AMTI (Airborne Moving Target Indication) to detect the aircraft.

L Band (from 1.0 to 2.0 GHz). The surveillance radars which are land-based and long-range are optimal in this frequency area, e.g. the 200 nmi radars used for the control of the air traffic. In this frequency area, it is feasible to obtain high power with narrow-beamwidth antennas and strong MTI performance. Low external noise is present. Large radars which must identify extraterrestrial targets at long-range use the L-band.

S Band (from 2.0 to 4.0 GHz). As noted in the previous frequency range, the surveillance radar may deal also with S-band, but long-range can be more challenging to achieve than lower frequencies. When a huge number of MTI radars arise as the frequency increase, some blind speeds occur and MTI are less adequate. A defect may occur with bad weather conditions (e.g. rains) since the range of S-band might be reduced, but this frequency area is the most used in weather radars. So, this band is the most common for long-range weather radars and it is also good for medium-range air surveillance applications (e.g. airport surveillance radar (ASR) in air terminals). Military 3D radars and height-finding radars are found in this frequency area, due to tighter beamwidths which supply good angular accuracy and resolution. Also, the main beam jamming can be reduced, in the military radar case. An important notice is the usage of this band also in the long-range airborne air surveillance pulse Doppler radars (e.g. Airborne Warning and Control System (AWACS)). Regarding frequency areas, the lower frequency band with respect to the ones of S-band is useful for air surveillance, but the higher frequency band are better for information gathering (i.e. the high data rate precision tracking). The S-band is also an optimal trade-off if a single frequency must be used for both air surveillance and precision tracking.

C Band (from 4.0 to 8.0 GHz). This frequency band is a good compromise between the S-band and the X-band. Long-range air surveillance radars do not perform in this frequency area, which is optimal for long-range precision instrumentation radars (e.g. the ones used for missile tracking). Multi-function phased array air defense radars and medium-range weather radars also use this frequency band.

X Band (from 8.0 to 12.5 GHz). Civil applications and military weapon control radars use this frequency area. In the X band the piloting and shipboard navigation, weather avoidance, Doppler navigation, and the radar speed gun work. The band is pretty large and it allows the generation of short pulses, the tight bandwidth obtained through small-size antennas, thus it is an advantage in information gathering and high-resolution radar cases.

$\mathbf{K_u}$, K and $\mathbf{K_a}$ Bands (from 12.5 to 40 GHz). In the beginning, the K-band radars were centered to a wavelength close to the resonance wavelength of water vapor, in which the absorption may reduce the radar range. So, the K-band has been split into two bands: $\mathbf{K_u}$ is the lower frequency band, $\mathbf{K_a}$ is the higher frequency band. A good reminder is the wide bandwidths and the tighter beamwidths, which may be obtained through small apertures. Dealing with higher frequencies, limitations due to rain clutter and attenuation are difficult. Some radars like the airport surface detection radar used to localization and control of ground traffic in the airports, use the lower frequency band ($\mathbf{K_u}$).

Millimeter Wavelengths (above 40 GHz). The millimeter-wave radars work in a frequency region between 40 and 300 GHz. Serious applications are not feasible around 60 GHz of frequency due to the high attenuation induced by the atmospheric oxygen absorption line. So, the 94 GHz frequency band is typically noted as the "normal" frequency regarding the millimeter radar. No radar, for years, has been produced above the $\mathbf{K_a}$ band. An important notice is that the propagation window at 94 GHz has a greater attenuation regarding the one at water-vapor absorption line at 22.2 GHz. The millimeter-wave region can be interesting in space applications, short-range applications within the atmosphere.

Laser frequencies. The usage of laser in the infrared, optical, and ultraviolet regions of the electromagnetic spectrum can provide coherent power of a great magnitude and efficiency, as well as tight directive beams. Lasers are optimal choices for target information-gathering applications because of their good angular resolution and range resolution. Measurements of profiles of atmospheric temperature, water vapor, and ozone, measurements of cloud height and of tropospheric wind are some examples of laser applications. The main fault of laser applications is the difficulty to operate in particular weather conditions, such as rain, clouds, or fog.

4.3 Radar tracking algorithms

Estimating the trajectory of a track starting from some measurements is a tracking problem. The process of track filtering is divided into: **track filtering** and **measurements-to-track data association**.

The **track filtering** approach involves the estimation of the trajectory (position, velocity, and sometimes acceleration) and the estimation of a track from measurements (range, bearing, elevation). To predict the next measurement, the position and velocity estimates are used.
The **measurements-to-track data association** involves assigning a measurement to an existing track or identifying a new target or a false signal.
Note that as measurements to the measurements-to-track data association and track filtering are matched the range estimation, the angle of arrival, and range rate [13].

4.3.1 Track filtering fundamentals

In the most used radar systems, the target motion is described in Cartesian coordinates, while the radar measurements are provided in polar or spherical coordinates. The basic idea is to filter the track by using the Cartesian coordinates, so the radar measurement is used as a linear observation of the corresponding kinematic state. The algorithms used for track filtering may be divided into two main groups: the first deals with a parametric estimation approach in which the model is assumed to be coherent with the target motion and the data distortion is predicted by using a consistent time period. The more the covariance drops to zero, the more the processing of new data will drop to zero. The second group deals with a stochastic state estimation approach which uses a non-perfect model for target motion. This non-perfect model depends on the use of a random process, which is not able to give an accurate estimation of the kinematic state [13].

4.3.2 Motion models

The state of a target is displayed in Cartesian coordinates in which the reference frame is relative to the platform space location. The equation which describes that target motion is:

$$\mathbf{x}_{k+1} = \mathbf{F}_k \mathbf{x}_k + \mathbf{G}_k \mathbf{v}_k \tag{4.26}$$

where $\mathbf{x}_k$ stands as the following state vector, in 2D

$$\mathbf{x}_k = [\mathbf{x}_k \quad \dot{\mathbf{x}}_k \quad \mathbf{y}_k \quad \dot{\mathbf{y}}_k]^T \tag{4.27}$$

where $(\mathbf{x}_k, \mathbf{y}_k)$ are the target positions, while $(\dot{\mathbf{x}}_k, \dot{\mathbf{y}}_k)$ are the target velocities. However the state vector may be a function of a 3D model, including also the $\mathbf{z}_k$ position and the $\dot{\mathbf{z}}_k$, but tracking with surveillance radars which measure only the range target and the bearing target the Cartesian space may be referred only to the main measurements $\mathbf{x}_k$ and $\dot{\mathbf{x}}_k$ [13].

4.3.3 Measurements models

The measurements coming from a radar system are polar or spherical. In most measurement cases, the radar computes the velocity of the target all along the range vector which stands between the target and the antenna. The measurement equation is:

$$\mathbf{z}_k = h_k(\mathbf{x}_k) + \mathbf{w}_k \tag{4.28}$$

where the $\mathbf{z}_k$ is the measurement vector at time t_k, and the $\mathbf{w}_k$ is the measurement error at time t_k ($\mathbf{w}_k \sim \mathbf{N}(\mathbf{0}, \mathbf{R}_k)$). The target state estimate is often retained in a Cartesian reference frame which is related to any motion of the radar antenna. To define a correlation between the two coordinate systems, an affine transform is sometimes used, so:

$$\mathbf{z}_k = h_k(\mathbf{M}_k\mathbf{x}_k + \mathbf{L}_k) + \mathbf{w}_k \tag{4.29}$$

where the $\mathbf{M}_k$ is the matrix that rotates the target state vector into the frame of the antenna at time t_k, and the $\mathbf{L}_k$ is the vector that translates the target state vector into the frame of the antenna at time t_k [13].

4.3.4 Radar track filtering

The estimation of the kinematic state of a target is done after the data identification and the assignment of a measurement to a track. The radar measurements are obtained in spherical or polar coordinates, while the target motion is described in Cartesian coordinates. Due to inaccurate results which may deal by converting the polar coordinates to the Cartesian ones, one of the methods to overcome this problem is to design an EKF to estimate the states. In this case, a parametric approach is used, and as more data are coming as more the state estimate covariance approaches zero. To use this approach the main methods are the nonlinear least square or the maximum likelihood estimation [13].

Extended Kalman Filter

The EKF is the nonlinear extension of the KF since in real-world applications the radar system must deal with nonlinear measurements. The measurement equation is the same as Equation 4.28, and the motion model is:

$$\mathbf{x}_{k+1} = \mathbf{F}_k\mathbf{x}_k + \mathbf{G}_k\mathbf{v}_k \tag{4.30}$$

where $\mathbf{G}_k$ is the input matrix at time t_k for target motion, the $\mathbf{v}_k$ is the white noise error ($\mathbf{v}_k \sim \mathbf{N}(\mathbf{0}, \mathbf{Q}_k)$). The EKF state prediction and state update are respectively:

State prediction:

$$\mathbf{x}_{k|k-1} = \mathbf{F}_{k-1}\mathbf{x}_{k-1|k-1} \tag{4.31}$$
$$\mathbf{P}_{k|k-1} = \mathbf{F}_{k-1}\mathbf{P}_{k-1|k-1}\mathbf{F}_{k-1}^T + \mathbf{G}_{k-1}\mathbf{Q}_{k-1}\mathbf{G}_{k-1}^T \tag{4.32}$$

State update:

$$\mathbf{x}_{k|k} = \mathbf{x}_{k|k-1} + \mathbf{K}_k\tilde{\mathbf{z}}_k \tag{4.33}$$
$$\tilde{\mathbf{z}}_k = \mathbf{z}_k - h_k(\mathbf{x}_{k|k-1}) \tag{4.34}$$
$$\mathbf{P}_{k|k} = [\mathbf{I} - \mathbf{K}_k\mathbf{H}_k]\mathbf{P}_{k|k-1} \tag{4.35}$$
$$\mathbf{K}_k = \mathbf{P}_{k|k}\mathbf{H}_k^T\mathbf{S}_k^{-1} \tag{4.36}$$
$$\mathbf{S}_k = \mathbf{H}_k\mathbf{P}_{k|k-1}\mathbf{H}_k^T + \mathbf{R}_k \tag{4.37}$$

The EKF does not give an optimal estimate of the target state, since the measurements are a nonlinear function of the target state and so, the filter deals with a linearized output matrix for $h_k(\mathbf{x}_k)$ in the covariance update. Usually, the target estimation state is retained in a Cartesian reference frame which is not affected by any motion of the radar antenna. An affine transformation is used to define a correlation between the two coordinate systems (see Equation 4.29). So the EKF measurement update is given by:

Update of the state estimate with the measurement:

$$\mathbf{x}_{k|k} = \mathbf{x}_{k|k-1} + \mathbf{K}_k[\mathbf{z}_k - h_k(\mathbf{M}_k\mathbf{x}_{k|k-1} + \mathbf{L}_k)] \tag{4.38}$$
$$\mathbf{P}_{k|k} = [\mathbf{I} - \mathbf{K}_k\mathbf{H}_k\mathbf{M}_k]\mathbf{P}_{k|k-1} \tag{4.39}$$
$$\mathbf{K}_k = \mathbf{P}_{k|k-1}\mathbf{M}_k^T\mathbf{H}_k^T\mathbf{S}_k^{-1} \tag{4.40}$$
$$\mathbf{S}_k = \mathbf{H}_k\mathbf{M}_k\mathbf{P}_{k|k-1}\mathbf{M}_k^T\mathbf{H}_k^T + \mathbf{R}_k \tag{4.41}$$

where:

$$\mathbf{H}_k = \left[\frac{\boldsymbol{\delta} h_k(\mathbf{x}_k)}{\boldsymbol{\delta}\mathbf{x}_k}\right]_{X_k = M_k x_{k|k-1} + L_k} \tag{4.42}$$

Converted Measurement Filter

About the Converted Measurement Filter, an important notice is the linear relationship between the state and the measurements. The measurement equation is a function of $\mathbf{z}_k$, when working with a converted measurement filter in Cartesian space:

$$\mathbf{z}_k = \begin{bmatrix} \mathbf{x}_k^m \\ \mathbf{y}_k^m \\ \mathbf{z}_k^m \end{bmatrix} = \begin{bmatrix} 1 & 0 & 0 & 0 & 0 & 0 \\ 0 & 0 & 1 & 0 & 0 & 0 \\ 0 & 0 & 0 & 0 & 1 & 0 \end{bmatrix} \mathbf{x}_k + \begin{bmatrix} \mathbf{w}_{xk} \\ \mathbf{w}_{yk} \\ \mathbf{w}_{zk} \end{bmatrix} = \mathbf{H}\mathbf{x}_k + \mathbf{W}_k \tag{4.43}$$

where:

- $\mathbf{x}_k^m$ is the measured $\mathbf{x}$ coordinate at time t_k;
- $\mathbf{y}_k^m$ is the measured $\mathbf{y}$ coordinate at time t_k;
- $\mathbf{z}_k^m$ is the measured $\mathbf{z}$ coordinate at time t_k;
- $\mathbf{w}_{xk}$ is the error in $\mathbf{x}$-coordinate at time t_k;
- $\mathbf{w}_{yk}$ is the error in $\mathbf{y}$-coordinate at time t_k;
- $\mathbf{w}_{zk}$ is the error in $\mathbf{z}$-coordinate at time t_k.

Note that the measurements $(\mathbf{x}_k^m, \mathbf{y}_k^m, \mathbf{z}_k^m)$ are calculated from the spherical or sine space measurements, while the measurements error $(\mathbf{w}_{xk}, \mathbf{w}_{yk}, \mathbf{w}_{zk})$ are cross-correlated and non-Gaussian. Due to this last feature, the Kalman filter is no longer the optimal choice.

4.4 Radar applications

Radar technology may be used for a huge array of remote sensing applications since its main goal is to search/detect, track, and image. Radar has a wide range of applications: ground-penetrating systems, in which the maximum range is a few meters, long-range-over-the-horizon search systems, which can identify targets many kilometers away, collision avoidance. Radar applications may be split into two categories: military and commercial/civil applications. However, some basic tasks are applied in both cases [13][14].

4.4.1 Civil applications

During the last decades, some experiments in the automotive field have been performed. The idea is to develop radar applications in the frequency 17 GHz, 24 GHz, 35 GHz, 49 GHz, 60 GHz, and 77 GHz. The goal is to avoid collisions between vehicles and to develop a field of automatic driving cars. Over the years significant expertise are acquired in the field of microwaves and radar signal processing. Between 1990 and 2000, the commercialization of automotive radar was possible by the significant improvements in semiconductor microwave sources and the accessible computation power of microcontrollers and digital signal processing units. The radar sensors are fundamental because of their potential detection of the surrounding environment. Future vehicles may be completely automated or at least highly automated due to the strong development of sensor technology. Radar sensors are surely one of the main factors in self-driving technology. The most popular radar sensor is the ultrasonic one, but there are several others radar [15][14].

Figure 4.1: Equipment for self-driving car. Author: Alena Nesterova, CC BY-SA 4.0.

Ultrasonic ranging

Via the transmitter, ultrasonic sensors generate mechanical waves which own a greater frequency than the range of audible sound waves for human hearing. The waves are acquired by the receiver after the reflection. The most used frequencies are 40 kHz, 48 kHz, and 58 kHz. When dealing with a high frequency, more sensor precision is obtained. The ultrasonic sensor may transmit the signal as rays because of the sensor's tiny diffraction and strong directivity. It is mostly employed in low-speed driving situations such as automatic parking radars.

Millimeter wave radar sensor

The millimeter wave radar sensor works at 30 $\sim$ 300 GHz. This radar has properties of both the infrared waves and the microwaves due to its long wavelength. It can adapt to different climatic situations since the wave is not vulnerable to external climatic conditions. By using measurement techniques, it is possible to separate the millimeter wave radar into pulse mode and frequency modulation continuous wave mode.

Light Detection and Ranging (LIDAR)

By emitting a laser beam, LIDAR is used to estimate the location of the target. This laser light is an electromagnetic wave, which is different from the mechanical waves. LIDAR has two scanning modes: two dimensions and three dimensions. The basic idea behind the measurement is to determine the distance by timing the interval between the laser's emission and the object's reflection. Notice that the more the number of radar mechanical structures decreases the more the radar reliability and integration increase.

Figure 4.2: Leica terrestrial LIDAR (light detection and ranging) scanner (TLS). Author: David Monniaux, CC BY-SA 3.0.

4.4.2 Military applications

Military systems are developed by the U.S. military arm for army equipment. The AN/xxx-nn is the used nomenclature. About the "xxx": the first letter stands for the installation type, the second letter indicates the equipment type, and the third letter designates the specific applications. The "nn" is a numerical sequence. Some examples of radars are: the AN/TQP-36 which is a ground-based transportable special purpose radar, the AN/SPY-1 used for surveillance and fire control radar (FCR) system [13].

Search Radars

Two independent radar systems are used to perform the search requirements and the track ones. This is the study case dealing with ground-based or surface ship systems, but sometimes some applications do not allow the use of multiple radars. Some examples of application radars which do not enhance the employment of two different radars are airborne application and electronically scanned antenna systems.

Two-Dimensional Search. Several volume search systems achieve the search using a "fan"-shaped antenna pattern, typically in the azimuth and range dimensions. Due to the antenna aperture, it will be horizontally large while vertically tiny, so the azimuth beamwidth results tight while the elevation beamwidth outcome is wide. An example of 2D radar is the AN/SPS-49, which is a 2D air search radar that operates in the UHF band (850-942 MHz). The AN/SPS-49 can acquire air targets in the sea due to its huge mechanically stabilized truncated parabolic antenna. This 2D radar has a good amount of features that enhance radar performance, such as clutter maps and automatic target detection with pulse-Doppler processing. In the last years, a new version of this radar (the SPS-49A (V)1) consists in an estimation of all the targets performing single-scan radial velocity. The beamwidths of SPS-49 are 3,3° in azimuth and 11° in elevation. The antenna may rotate at 6 rmp or 12 rmp, and rmp stands for "revolution per minute". The radar may also operate in both large-range and short-range mode. Dealing with the long-range small target at around 200 miles may be detected, while regarding the short-range mode, low-flying targets and missiles may be detected.

Three-Dimensional Search. The 3D search radar has multiple examples of applications and used technologies. The AN/SPS-48, which was produced by ITT Gilfillan, has a square planar array as antenna which is based on a slotted waveguide. A serpentine structure stuck with the planar array is supplying the antenna. The frequency sensitivity able to elevation scanning is supplied by the serpentine. The scanning of the radar is performed in elevation, by an angle up to 65°. The reference frequency area of the AN/SPS-48 is the S-band (2 GHz - 4 GHz) considering an average rated power of 35 kW. The combat system of some shipboards holds control of the SPS-48, and provides measurements like range, azimuth, elevation, and speed. It is a very good radar in the defense area.

Figure 4.3: An AN-SPS/49 radar on USS Abraham Lincoln. Author: Don S. Montgomery, USN (Ret.), public domain.

Figure 4.4: An AN-SPS/48 radar on USS Theodore Roosvelt. Author: PH2 Tracy Lee Didas, public domain.

Air Defense Radars

Two main examples are reported. The AN/TPS-75 has functionality very similar to the 3D radars. Frequency scanning is the essential method to compute mechanically the azimuth direction and electronically the elevation dimension. This radar is based on a long and tiny antenna that investigates the observed target to obtain an IFF response. In the interest of IFF interrogation to occur quickly following target detection while the antenna spins in azimuth, the IFF antenna angle stands a bit back with respect to the azimuth one. An important notice is the different position of the IFF antenna angle rather than the one of azimuth, since the IFF examination may occur not long after the target identification while the antenna rotates in azimuth. The AN/MPQ-64 Sentinel is provided to the U.S. Army and U.S. Marine Corps. This radar is an X-band system used when airborne dangers follow. The system is used to detect, track and identification of airborne threats.

Figure 4.5: An AN-TPS/75 radar. Author: Steve Grzezdzinski, public domain.

Over-the-Horizon Search Radars

The goal of the design of the Over-the-Horizon (OTH) search radar is to detect ballistic missiles which are located many miles away. These radars use the ionosphere's refractive effect to identify objects located at long range. Furthermore, the OTH's frequency stands in HF band (3 MHz - 30 MHz). Due to the need to have a tight beamwidth, dealing with low frequencies the antenna must be very large.

Figure 4.6: An OTH radar station. Author: US Navy, public domain.

Figure 4.7: US Navy Relocatable Over-the-Horizon radar station. Author: US Navy, public domain.

Chapter 5

EKF and DVS implementation

The main idea of this thesis is to design a DVS and an EKF to estimate target trajectory by using radar measurements. Then, the obtained performances in terms of RMSE are compared, and the best method is highlighted. To navigate all around the possible location of the target, multiple data sets (reference data) are initialized. Designing a proper model means dealing with a good amount of data sets. An amount of 25 data sets (**identification data sets**) are initialized, the first 15 sets are generated using a random wave, while the final 10 sets are generated using a sine wave. The random wave is the most used due to its capability to be able to seize a larger domain in the space. The two-step procedure is pursued by designing an Extended Kalman Filter using the proper Simulink block (see Section 5.4). Instead, the one-step approach is performed by designing a Direct Virtual Sensor using the System Identification Toolbox by merging the 25 data sets previously obtained. Then, after properly obtaining an optimal EKF model and the best DVS model (linear or nonlinear), the performances in terms of RMSE are compared by using a different 20 data sets (**validation data sets**) (see Section 5.5).

5.1 Main model for radar localization systems

A target is usually managed as a point object without a shape in tracking, mainly in target dynamic models. The most used maneuvering target tracking methods assume that the target motion and its observations can be stated as known mathematical models. So, the state-space model is:

$$\dot{\mathbf{x}}_{k+1} = f_k(\mathbf{x}_k, \mathbf{u}_k) + \mathbf{w}_k \tag{5.1}$$
$$\mathbf{z}_k = h(\mathbf{x}_k) + \mathbf{v}_k \tag{5.2}$$

where $\mathbf{x}_k$ is the target state, $\mathbf{z}_k$ is the observation, $\mathbf{u}_k$ is the control input vector and they are computed in discrete time t_k; $\mathbf{w}_k$ is the process noise sequence and $\mathbf{v}_k$ is the measurement noise sequence. Finally, the f_k and h_k are the vector value functions. Note that usually a **discrete-time** system is derived dealing with target tracking, by discretizing the following **continuous-time** system:

$$\dot{\mathbf{x}}(t) = f(\mathbf{x}(t), \mathbf{u}(t), t) + \mathbf{w}(t) \tag{5.3}$$

$$\mathbf{z}(t) = h(\mathbf{x}(t), t) + \mathbf{v}(t) \tag{5.4}$$

Some basic assumptions related to the previous system are:

- $\mathbf{x}_k = \mathbf{x}(t_k)$;
- $\mathbf{z}_k = \mathbf{z}(t_k)$;
- $\mathbf{v}_k = \mathbf{v}(t_k)$;
- $h_k(\mathbf{x}_k) = h(\mathbf{x}(t_k), t_k)$;
- The control input is assumed to be piece-wise constant, so $\mathbf{u}_k = \mathbf{u}(t)$;
- The time term $t_k \leq t < t_{k+1}$.

When approaching target tracking the input $\mathbf{u}$ is usually not known. Furthermore, it is relevant to state the following equation system:

$$\mathbf{w}_k \neq \mathbf{w}(t_k) \tag{5.5}$$

$$f_k(\mathbf{x}_k, \mathbf{u}_k, \mathbf{w}_k) \neq f(\mathbf{x}(t_k), \mathbf{u}(t_k), \mathbf{w}(t_k), t_k) \tag{5.6}$$

A 2D scenario, in which the altitude $\mathbf{z}$ is not considered, may be depicted considering the following models:

$$\dot{\mathbf{x}}(t) = \mathbf{A}_{CV}\mathbf{x}(t) + \mathbf{B}_{CV}\mathbf{w}(t) \tag{5.7}$$

$$\mathbf{x}_{k+1} = \mathbf{F}_{CV}\mathbf{x}_k + \mathbf{G}_{CV}\mathbf{w}_k \tag{5.8}$$

$$\mathbf{x}_{k+1} = \mathbf{F}_{CV}\mathbf{x}_k + \mathbf{w}_k \tag{5.9}$$

The above models are known as the continuous-time, discrete-time, and **constant velocity (CV)** models. CV models are so named since the accelerations along x and along y are not declared but are noted as Gaussian white noise terms. When is unnecessary, an optimal choice is to not include some components in the state vector (e.g. accelerations), since the tracking performance may degrade [16]. The state vector form in the 2D scenario is:

$$\begin{aligned}\mathbf{x}(t) &= [\mathbf{x}_1(t), \mathbf{x}_2(t), \mathbf{x}_3(t), \mathbf{x}_4(t)] \\ &= [\mathbf{x}(t), \dot{\mathbf{x}}(t), \mathbf{y}(t), \dot{\mathbf{y}}(t)],\end{aligned} \tag{5.10}$$

In Equation 5.10, the terms $\mathbf{x}(t)$, $\mathbf{y}(t)$ are the Cartesian coordinates used to describe the motion of the system [1]. The state equations are:

$$\left.\begin{aligned}\dot{\mathbf{x}}_i(t) &= \mathbf{x}_{i+1}(t)\\ \dot{\mathbf{x}}_{i+1}(t) &= \mathbf{v}_i(t)\end{aligned}\right\}\text{for i = 1,3} \tag{5.11}$$

5.2 Target dynamics

The 2 dimensions ($\mathbf{x}$ and $\mathbf{y}$) target tracking assumes constant velocities in the respective dimensions (CV models). So, the state vector $\mathbf{x}_n$ contains 4 variables:

$$\mathbf{x}_n = [\mathbf{x}_n, \mathbf{y}_n, \mathbf{v}_{x,n}, \mathbf{v}_{y,n}]^T \tag{5.12}$$

In the state vector (Equation 5.12), $\mathbf{x}_n$ and $\mathbf{y}_n$ are the positions of the target, while $\mathbf{v}_{x,n}$ and $\mathbf{v}_{x,n}$ are the velocities of the target. So, the discretized motions equations are:

$$\begin{bmatrix}\mathbf{x}_{n+1}\\ \mathbf{y}_{n+1}\\ \mathbf{v}_{x,n+1}\\ \mathbf{v}_{y,n+1}\end{bmatrix} = \begin{bmatrix}1 & 0 & T_s & 0\\ 0 & 1 & 0 & T_s\\ 0 & 0 & 1 & 0\\ 0 & 0 & 0 & 1\end{bmatrix}\begin{bmatrix}\mathbf{x}_n\\ \mathbf{y}_n\\ \mathbf{v}_{x,n}\\ \mathbf{v}_{y,n}\end{bmatrix} + \begin{bmatrix}T_s^2/2 & 0\\ 0 & T_s^2/2\\ T_s & 0\\ 0 & T_s\end{bmatrix}\begin{bmatrix}\mathbf{a}_{x,n}\\ \mathbf{a}_{y,n}\end{bmatrix} \tag{5.13}$$

The vector $[\mathbf{a}_{x,n}, \mathbf{a}_{x,n}]^T$ is composed of the two terms stationary Gaussian random distributed with zero-mean and well-known variance. The T_s is the sampling time, while the accelerations in $\mathbf{x}$ and $\mathbf{y}$ coordinates are mutually statistically independent. Equation 5.13 may be stated in matrix notation:

$$\mathbf{x}_{n+1} = \mathbf{F}\mathbf{x}_n + \mathbf{G}\mathbf{v}_n \tag{5.14}$$

where $\mathbf{x}_{n+1}$ is the next step-state vector, $\mathbf{F}$ is the transition matrix, $\mathbf{x}_n$ is the state vector, $\mathbf{G}$ is the noise gain matrix and $\mathbf{v}_n$ is the noise process sequence with zero-mean and covariance $\mathbf{Q}_d$.

5.3 Radar measurements

Using a radar to compute the position of a target in 2D space, the measurements are got in spherical or polar coordinates, the range and the azimuth. The relation between the polar coordinates and the Cartesian ones is reported below:

$$\begin{bmatrix}\mathbf{r}_n\\ \boldsymbol{\theta}_n\end{bmatrix} = \begin{bmatrix}\sqrt{\mathbf{x}_n^2 + \mathbf{y}_n^2}\\ \mathbf{arctan}(\mathbf{y}_n/\mathbf{x}_n)\end{bmatrix} + \begin{bmatrix}\mathbf{w}_{r,n}\\ \mathbf{w}_{\theta,n}\end{bmatrix} \tag{5.15}$$

where $\mathbf{r}_n$ and $\boldsymbol{\theta}_n$ are the measured range and azimuth, the $\mathbf{x}_n$ and $\mathbf{y}_n$ are the states which correspond to the respective position and $\mathbf{w}_{r,n}$ and $\mathbf{w}_{\theta,n}$ are the white Gaussian measurement noise. Note that, the range and the azimuth are uncorrelated and they are corrupted by a noise covariance $\mathbf{R}_d$. The matrix notation of Equation 5.15 is:

$$\mathbf{z}_n = h(\mathbf{x}_n) + \mathbf{w}_n \tag{5.16}$$

where $\mathbf{z}_n$ is the polar coordinates vector, $h(\cdot)$ is the transformation from Cartesian to polar coordinates and $\mathbf{w}_n$ is the zero-mean white Gaussian noise.

5.4 Two-step approach: design of Extendend Kalman Filter (EKF)

To estimate the states of the discrete-time nonlinear system, the EKF Simulink block depicted in Figure 5.1 is used.

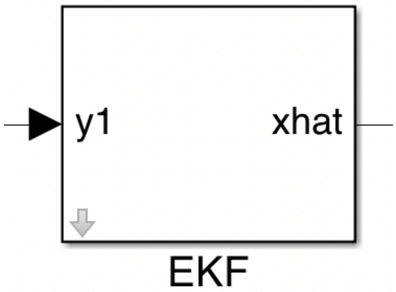

Figure 5.1: The Extended Kalman Filter block used in Simulink.

Using the state transition function and the measurement functions of the nonlinear system and the basic Extended Kalman filter algorithm, this Simulink block produces the state estimates $\hat{\mathbf{x}}$, referred to current time step.
The used state transition function is described below and the process noise covariance is $\mathbf{Q}_d$, specified as a diagonal matrix $\mathbf{N}_s - by - \mathbf{N}_s$, where $\mathbf{N}_s$ is the number of states of the system.

Listing 5.1: State transiction function.

```
function stateNext = stateModel(state)
    dt = 0.2;
    F = [1 0 dt 0;
        0 1 0 dt;
        0 0 1 0;
        0 0 0 1];
    stateNext = F*state;
```

The built measurement function is depicted below and the measure noise covariance is $\mathbf{R}_d$.

Listing 5.2: Measurement function.

```
function z = measureModel(state)
    angle = atan(state(2)/state(1));
    r = norm([state(1:2)]);
    z = [angle;r];
```

The estimated state is so obtained from the block and the state of motion of a detected object is known. To better evaluate the truth of the obtained value and the consistency of the estimated states with respect to the nominal ones, a comparison between the two is performed. In the following figures, using both a random wave and a sine wave as a reference, the true trajectory and the estimated trajectory are compared.

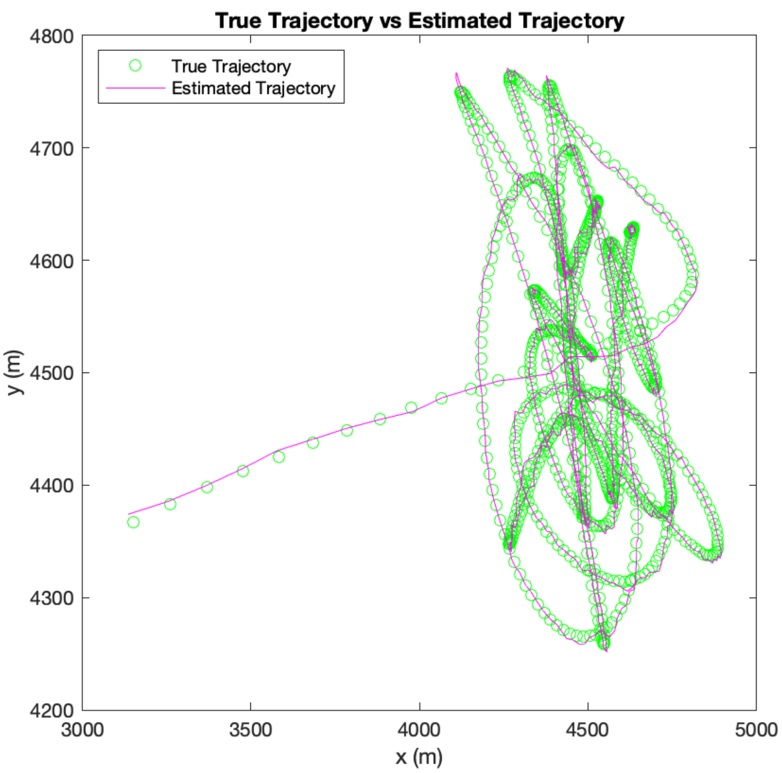

Figure 5.2: Comparison of trajectories using a random wave reference.

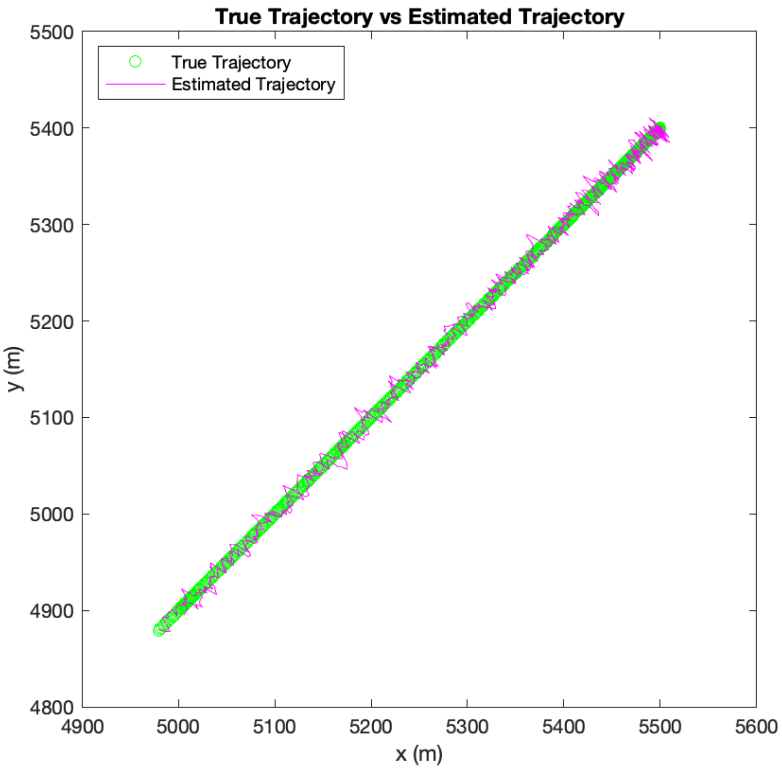

Figure 5.3: Comparison of trajectories using a sine wave reference.

5.5 One-step approach: design of Direct Virtual Sensor design (DVS)

The DVS design involves the identification of a model directly using data sets. To estimate such a model, the System Identification Toolbox in MATLAB is used. After importing the identification data sets, the 25 data sets are merged to properly obtain an optimal model. The aim is to obtain the simpler and the best model to compare the obtained performances with the ones obtained by estimating an EKF. In the trial and error procedure, primarily some linear (polynomial) models (ARX, ARMAX, OE) are estimated. An initial screening of the accuracy of the model may be done by evaluating the best-fit parameter of the respective model. This screening is useful to discard the non-coherent models. Unfortunately, no polynomial models overcome the first screening. Then, some nonlinear ARX models are designated. In the identification settings, it is possible to modify the number of terms of input and output channels and to choose the type of nonlinearity (see Section 5.6). The choice is to only deal with sigmoid networks as nonlinearity. In the first step, some NARX models are designated and, as the previous computation on polynomial models, a trial and error procedure, by adjusting and increasing the number of terms in the regressors and the number of units in the nonlinear block, is performed. From the best-fit values, some models seem to be coherent, so they are imported in Simulink area and model validation is executed. To validate such a model, validation data sets are gathered. Since those NARX do not give good results in terms of performance, another trial and error procedure is performed, and the obtained best estimator is a non-autoregressive NARX. In Figure 5.4 and in Figure 5.5 the measured and simulated model output is reported, while in Figure 5.6 and in Figure 5.7 some details are highlighted. The mentioned figures refer to the best estimator in the **x position**. In Section 6.2 the optimal filter features are well explained.

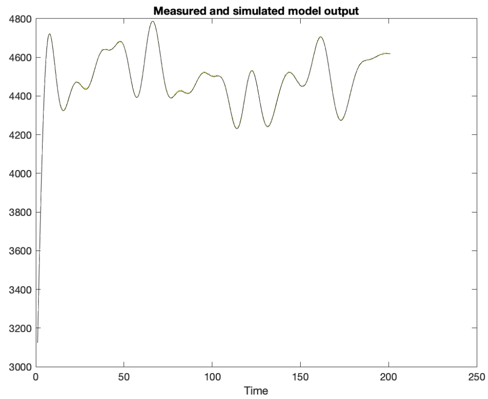

Figure 5.4: Model output of the **x position** considering a random wave.

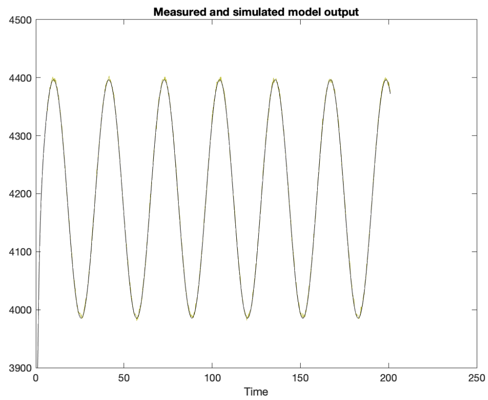

Figure 5.5: Model output of the **x position** considering a sine wave.

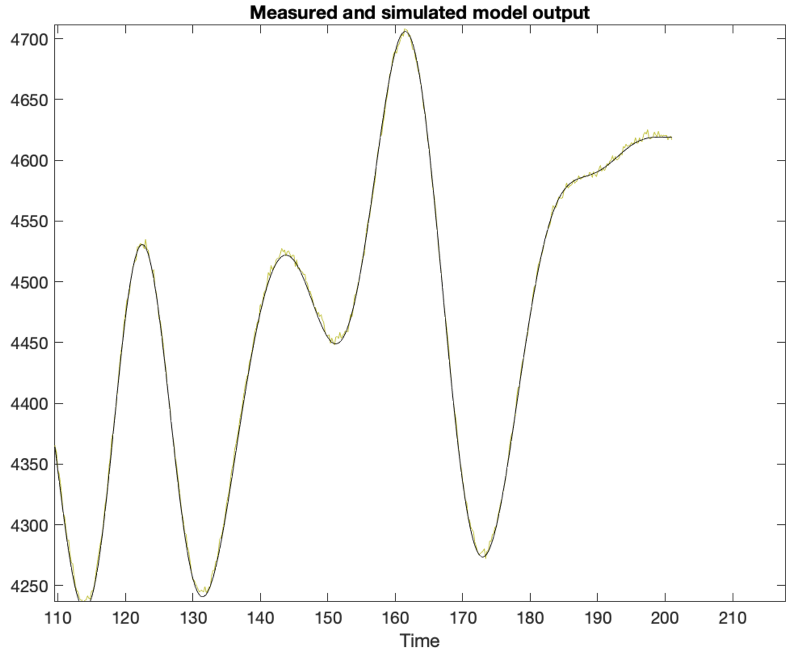

Figure 5.6: Detail of model output of the **x position** considering a random wave.

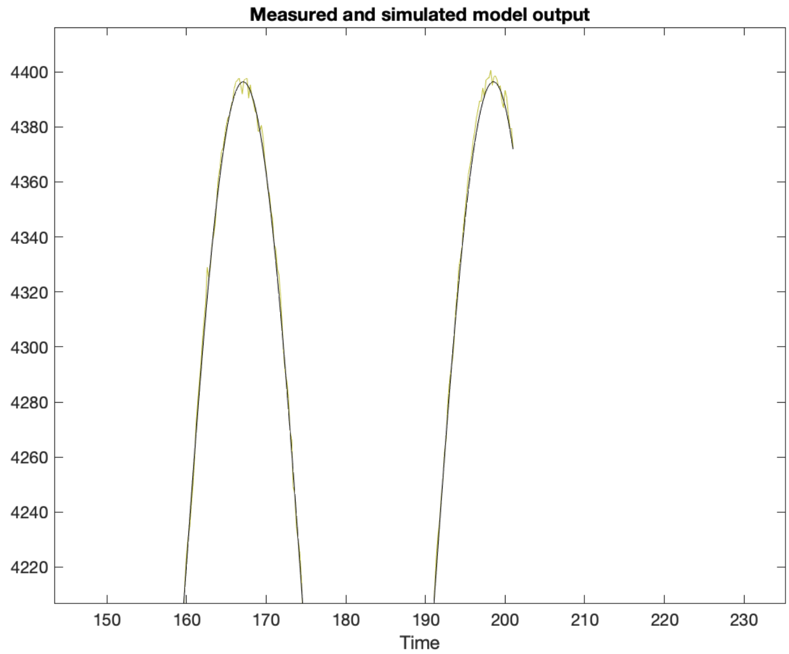

Figure 5.7: Detail of model output of the **x position** considering a sine wave.

5.6 NARX structure and neural networks

Nonlinear ARX models (NARX) are the nonlinear extension of the linear ARX models. To design these models, flexible nonlinear functions are used [17]. To compute the nonlinear ARX model it is useful to start approaching the linear SISO ARX model, which has the following structure:

$$\begin{aligned} &\mathbf{y}(t) + \mathbf{a}_1\mathbf{y}(t-1) + \mathbf{a}_2\mathbf{y}(t-2) + \dots + \mathbf{a}_{n_a}\mathbf{y}(t-n_a) = \\ &= \mathbf{b}_1\mathbf{u}(t) + \mathbf{b}_2\mathbf{u}(t-1) + \dots + \mathbf{b}_{n_b}\mathbf{u}(t-n_b+1) + \mathbf{e}(t) \end{aligned} \tag{5.17}$$

where $\mathbf{u}$ is the input, $\mathbf{y}$ is the output and $\mathbf{e}$ is the noise. From Equation 5.17, the current output $\mathbf{y}(t)$ is the predicted term according to the weighted sum of past output values and current and past input values. So, referring to Equation 5.17, the $\mathbf{n}_a$ is the terms of the past outputs, while the $\mathbf{n}_b$ is the past input terms used to predict the current output. The last equation may be detailed as:

$$\begin{aligned} &\mathbf{y}_p(t) = [-\mathbf{a}_1, -\mathbf{a}_2, \dots, -\mathbf{a}_{n_a}, \mathbf{b}_1, \mathbf{b}_2, \mathbf{b}_{n_b}] \cdot \\ &\cdot [\mathbf{y}(t-1), \mathbf{y}(t-2), \dots, \mathbf{y}(t-n_a), \mathbf{u}(t), \mathbf{u}(t-1), \dots, \mathbf{u}(t-n_b-1)]^T \end{aligned} \tag{5.18}$$

where $\mathbf{y}(t-1), \mathbf{y}(t-2), \dots, \mathbf{y}(t-n_a), \mathbf{u}(t), \mathbf{u}(t-1), \dots, \mathbf{u}(t-n_b-1)$ are the **regressor** terms. To compute a nonlinear ARX model:

- A more flexible function F is used instead of the weighted sum of the regressor terms:

  $$\mathbf{y}_p(t) = \mathbf{F}(\mathbf{y}(t-1), \mathbf{y}(t-2), \mathbf{y}(t-3), \dots, \mathbf{u}(t), \mathbf{u}(t-1), \mathbf{u}(t-2), \dots) \tag{5.19}$$

  $\mathbf{F}$ may represent one of the nonlinear functions explicated in the next paragraphs;

- The regressors of the nonlinear ARX models may be both input-output variables and nonlinear expressions of delayed input and output variables.

The structure of nonlinear ARX models is based on a block containing the regressor terms and an output function, which may hold **mapping objects** for each model output. Note that the output of the function block may state one or more mapping objects, so it is described as:

$$\mathbf{F}(\mathbf{x}) = \mathbf{L}^T(\mathbf{x} - \mathbf{r}) + g(\mathbf{Q}(\mathbf{x} - \mathbf{r})) + d \tag{5.20}$$

where $\mathbf{x}$ is the regression vector, $\mathbf{L^T}(\mathbf{x} - \mathbf{r})$ is the block output of linear function one, $g(\mathbf{Q}(\mathbf{x} - \mathbf{r}))$ is the output of the nonlinear function block, $\mathbf{r}$ is the vector of the regressor mean, $\mathbf{Q}$ is a projection matrix and d is the scalar offset.
$g(\mathbf{x})$ is a function like a sum of n units, nonlinear [18]:

$$g(\mathbf{x}) = \sum_{k=1}^{n} \boldsymbol{\alpha}_k \boldsymbol{\kappa}(\boldsymbol{\beta}_k^T(\mathbf{x} - \boldsymbol{\gamma}_k)) \tag{5.21}$$

where:

- $\boldsymbol{\beta}_k$ is a vector, so $\boldsymbol{\beta}_k^T(\mathbf{x} - \boldsymbol{\gamma}_k)$ is a scalar;
- $\boldsymbol{\kappa}$ is representing a function.

An example of $\boldsymbol{\kappa}(s)$ is the unit step function:

$$\boldsymbol{\kappa}(x) = \begin{cases} 0 & \text{for } \mathbf{x} < 0 \\ 1 & \text{for } \mathbf{x} \geq 0 \end{cases} \tag{5.22}$$

Regarding the step function in Equation 5.22, a smooth step, like **Sigmoid Function** can be initialized:

$$\boldsymbol{\kappa}(s) = \frac{\mathbf{1}}{\mathbf{1} + \mathbf{e}^{-s}} \tag{5.23}$$

However, the form of $\mathbf{F}(\mathbf{x})$ depends on the chosen mapping objects.

5.6.1 One layer sigmoid network

A sigmoid network function is implemented by a **idSigmoidNetwork** object. The network function operates on a ridge combination of inputs: $\mathbf{x}(t) = [\mathbf{x}_1(t), \mathbf{x}_2(t), \dots, \mathbf{x}_m(t)]^T$ which are mapped to a scalar output $\mathbf{y}(t)$:

$$\mathbf{y}(t) = \mathbf{y}_0 + (\mathbf{x}(t) - \overline{\mathbf{x}})^T \mathbf{PL} + \mathbf{S}(\mathbf{x}(t)) \tag{5.24}$$

where:

- $\mathbf{x}(t) \in \mathcal{R}^m$ is the vector of regressors with mean $\overline{x}$;
- $\mathbf{y}_0 \in \mathcal{R}$ is scalar offset;
- $\mathbf{P} \in \mathcal{R}^{m,p}$, $m \geq p$ is a projection matrix (p is the number of linear weights);
- $\mathbf{L} \in \mathcal{R}^p$ is a vector of weights;
- $\mathbf{S}(\mathbf{x})$ is a sum of dilated and translated sigmoid functions:

$$\mathbf{S}(\mathbf{x}) = \sum_{i=1}^{n} \mathbf{s}_i f((\mathbf{x} - \overline{\mathbf{x}})^T \mathbf{Q} \mathbf{b}_i + \mathbf{c}_i) \tag{5.25}$$

  where:

  - n is the number of units;
  - $\mathbf{Q} \in \mathcal{R}^{m,q}$, $m \geq q$ is a projection matrix;
  - the $\mathbf{s}_i \in \mathcal{R}$ are the output coefficients;
  - the $\mathbf{b}_i \in \mathcal{R}^q$ are the dilatation coefficients;
  - the $\mathbf{c}_i \in \mathcal{R}$ are the translations;
  - $f(z)$ is the sigmoid functions as defined above.

5.6.2 Wavelet network

A wavelet network function is implemented by a **idWaveletNetwork** object. The network function operates on radial combination of inputs: $\mathbf{x}(t) = [\mathbf{x}_1(t), \mathbf{x}_2(t), \ldots, \mathbf{x}_m(t)]^T$ which are mapped to a scalar output $y(t)$:

$$\mathbf{y}(t) = \mathbf{y}_0 + (\mathbf{x}(t) - \overline{\mathbf{x}})^T \mathbf{PL} + \mathbf{W}(\mathbf{x}(t)) + \mathbf{S}(\mathbf{x}(t)) \tag{5.26}$$

where:

- $\mathbf{x}(t) \in \mathcal{R}^m$ is the vector of regressors with mean $\overline{x}$;
- $\mathbf{y}_0 \in \mathcal{R}$ is scalar offset;
- $\mathbf{P} \in \mathcal{R}^{m,p}$, $m \geq p$ is a projection matrix (m is the number of regressors p is the number of linear weights);
- $\mathbf{L} \in \mathcal{R}^p$ is a vector of weights;
- $\mathbf{W}(\mathbf{x})$ is a sum of dilated and translated wavelets:

  $$\mathbf{W}(\mathbf{x}) = \sum_{i=1}^{d_w} \mathbf{w}_i f_w(\mathbf{b}i(\mathbf{x} - \overline{\mathbf{x}})^T \mathbf{Q} - \mathbf{c}_i) \tag{5.27}$$

  where:

  - $\mathbf{Q} \in \mathcal{R}^{m,q}$, $m \geq q$ is a projection matrix;
  - the $\mathbf{w}_i \in \mathcal{R}$ are the wavelet coefficients;
  - the $\mathbf{b}_i \in \mathcal{R}$ are the wavelet dilations;
  - the $\mathbf{c}_i \in \mathcal{R}^q$ are the wavelet translations;
  - $f_w(x) = e^{xx^T/2}$ is the radial function.

- $\mathbf{S}(\mathbf{x})$ is a sum of dilated and translated scaling functions:

  $$\mathbf{S}(\mathbf{x}) = \sum_{i=1}^{d_s} \mathbf{s}_i f_s(\mathbf{b}i(\mathbf{x} - \overline{\mathbf{x}})^T \mathbf{Q} - \mathbf{e}_i) \tag{5.28}$$

  where:

  - $\mathbf{Q} \in \mathcal{R}^{m,q}$, $m \geq q$ is a projection matrix;
  - the $\mathbf{s}_i \in \mathcal{R}$ are the scaling coefficient;
  - the $\mathbf{b}_i \in \mathcal{R}$ are the scaling dilations;
  - the $\mathbf{e}_i \in \mathcal{R}^q$ are the translations;
  - $f(z)$ is the sigmoid functions as defined above.

5.6.3 Tree partition

A tree-partitioned nonlinear function is implemented by a **idTreePartition** object. The network function operates on radial combination of inputs: $\mathbf{x}(t) = [\mathbf{x}_1(t), \mathbf{x}_2(t), \ldots, \mathbf{x}_m(t)]^T$ which are mapped to a scalar output $\mathbf{y}(t)$.
The function $\mathbf{F}(\mathbf{x})$ is explained in 5.29.

$$\mathbf{F}(\mathbf{x}) = \mathbf{x}\mathbf{L} + [\mathbf{1}, \mathbf{x}]\mathbf{C_k} + d \tag{5.29}$$

where:

- $\mathbf{x}$ belongs to the partition $\mathbf{P_k}$
- $\mathbf{L} \in \mathcal{R}^m$
- $\mathbf{C}_k \in \mathcal{R}^{m+1}$
- $\mathbf{P}_k$ is a partition of the $x - space$

Note that the mapping of $\mathbf{F}$ is computed as:

1. Given the value of $\mathbf{J}$, it is initialized a dyadic tree with $\mathbf{J}$ levels and $N = 2^{J-1}$;
2. Each node at level $1 < j < J$ has two descendants at level $j+1$ and one parent at level $j-1$:
   - The root node at level 1 has two descendants;
   - Nodes at level $\mathbf{J}$ are terminating leaves of the tree and have one parent.
3. One partition element is associated with each node k of the tree:
   - Using the observations on the partition element $\mathbf{P}_k$, the vector of coefficient $\mathbf{C}_k$ is computed;
   - The partition element $\mathbf{P}_k$ is cut into two to obtain the partition elements of descendant elements when the node k is not a terminating node.
4. When the value of the mapping $\mathbf{F}$ is computed at $\mathbf{x}$, an adaptive algorithm selects the active node $\mathbf{k}$ of the tree.

Chapter 6

Simulations

6.1 Use of an optimal control LQR

Dealing with target tracking means trying to give an estimate of the target trajectory. This can be a difficult task, and so to try to restrict the target's region a control technique is implemented. A Linear-Quadratic Regulator (**LQR**) is designed. Dealing with discrete-time systems the LQR computes the state-feedback control:

$$\mathbf{u}_n = -\mathbf{K}\mathbf{x}_n \tag{6.1}$$

which minimizes the following cost function:

$$\mathbf{J} = \sum_{n=0}^{\infty} \mathbf{x}^T\mathbf{Q}\mathbf{x} + \mathbf{u}^T\mathbf{R}\mathbf{u} + \mathbf{2}\mathbf{x}^T\mathbf{N}\mathbf{u} \tag{6.2}$$

related to the system dynamics:

$$\mathbf{x}_{n+1} = \mathbf{A}\mathbf{x}_n + \mathbf{B}\mathbf{u}_n \tag{6.3}$$

In Figure 6.1 is well explained the usage of the LQR controller:

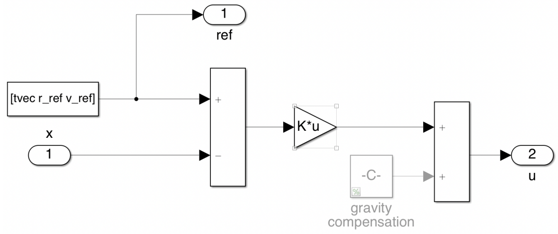

Figure 6.1: Controller implentation in Simulink.

In the studied case:

$$\mathbf{A} = \begin{bmatrix} 0 & 0 & 1 & 0 \\ 0 & 0 & 0 & 1 \\ 0 & 0 & 0 & 0 \\ 0 & 0 & 0 & 0 \end{bmatrix} \tag{6.4}$$

$$\mathbf{B} = \begin{bmatrix} 0 & 0 \\ 0 & 0 \\ 1 & 0 \\ 0 & 1 \end{bmatrix} \tag{6.5}$$

$$\mathbf{Q} = \begin{bmatrix} 10 & 0 & 0 & 0 \\ 0 & 10 & 0 & 0 \\ 0 & 0 & 10 & 0 \\ 0 & 0 & 0 & 10 \end{bmatrix} \tag{6.6}$$

$$\mathbf{R} = \begin{bmatrix} 0.1 & 0 \\ 0 & 0.1 \end{bmatrix} \tag{6.7}$$

6.2 Simulation results

The considered case refers to a NARX model with the following assumptions:

- Using sigmoid networks as nonlinearity, the number of units used in the nonlinear block is 30;
- In standard regressors bot input channels has 28 terms, while the output channel has 0 terms.

As noted in the above model settings, a non-autoregressive NARX is the right choice, by imposing 0 on the number of regressors of the output channel. Since the usual NARX models identified are not optimal to reach the goal, a non-autoregressive model is the optimal final choice. The RMSE values obtained from designing a DVS and an EKF are depicted in the tables below, in particular:

- In Table 6.1 there is the RMSE comparison referring to the position $\mathbf{x}$;
- In Table 6.2 there is the RMSE comparison referring to the position $\mathbf{y}$;
- In Table 6.3 there is the RMSE comparison referring to the position $\mathbf{v}_x$;
- In Table 6.4 there is the RMSE comparison referring to the position $\mathbf{v}_y$;

Notice that the used **multiple validation data set** is the same in estimating both the performances coming from position and velocities.

In Table 6.1, the obtained performances by stating the **x position** are depicted. An overall of 20 multiple validation data sets are initialized. Some random waves and sine waves are used as reference functions in the validation data set. From the obtained values there is evidence of a small improvement while using the DVS instead of the EKF. The worst and the best case are illustrated below:

Worst case. In the worst case, an enhancement of 0,1312 meters is gained.

Best case. In the best case, an enhancement of 1,2421 meters is gained.

By estimating the average of percentage error of best cases, an improvement of 28% is obtained. This is a very good result when dealing with small RMSE values. To better validate the models, different amplitude, bias, and frequency values are used while stating the reference functions.

Reference number	Reference type	EKF RMSE	DVS RMSE
1	Random wave	4.4249	3.3132
2	Random wave	4.7231	4.2089
3	Random wave	4.6492	4.2167
4	Random wave	4.6800	4.2126
5	Random wave	4.0649	3.2740
6	Random wave	4.1099	3.6965
7	Random wave	4.0566	3.8680
8	Random wave	4.7352	4.2082
9	Random wave	4.7093	4.2099
10	Random wave	4.6920	4.2124
11	Sine wave	4.4748	3.2327
12	Sine wave	4.5614	4.4125
13	Sine wave	4.4822	3.2601
14	Sine wave	4.4320	3.8916
15	Sine wave	4.5382	3.3247
16	Sine wave	4.4921	3.3191
17	Sine wave	4.4962	3.4049
18	Sine wave	4.5591	4.4279
19	Sine wave	4.5253	3.7192
20	Sine wave	4.5393	3.9260

Table 6.1: List of the 20 RMSE values obtained from EKF computation and DVS computation of **position x**.

Two charts are represented to better figure out the obtained RMSE values, referred to the **x position** and coming from the design of the EKF and the DVS. The orange lines are the RMSE amounts obtained from the EKF design, while the blue lines are the RMSE amounts coming from the DVS design. The overall RMSE measurements coming from the DVS design are lower (and so, better) than the ones coming from the EKF design.

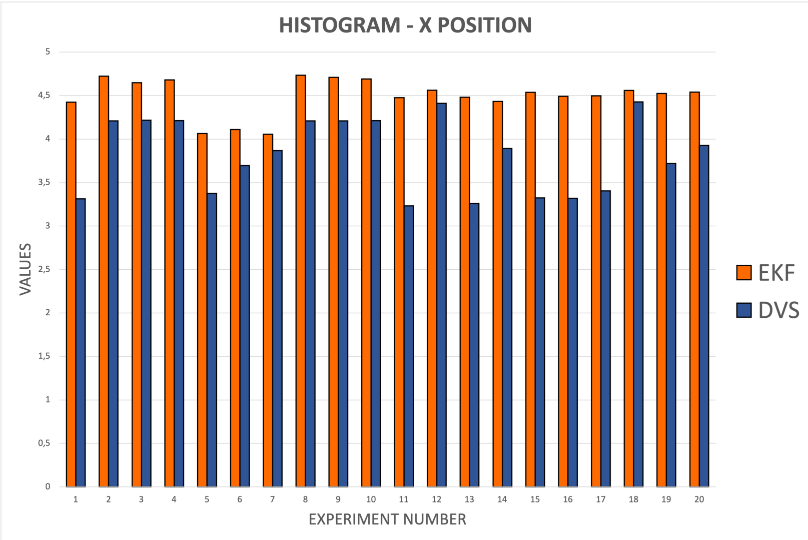

Figure 6.2: Histogram of RMSE values referred to the **x position**.

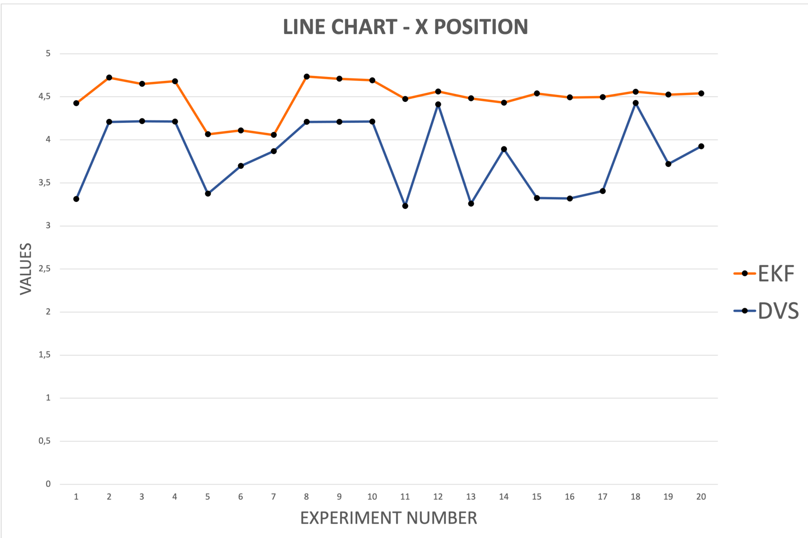

Figure 6.3: Line chart of RMSE values referred to the **x position**.

In Table 6.2, the obtained performances by stating the **y position** are depicted. An overall of 20 multiple validation data sets are initialized. Some random waves and sine waves are used as reference functions in the validation data set. From the obtained values there is evidence of a small improvement while using the DVS instead of the EKF. The worst and the best case are illustrated below:

Worst case. In the worst case, an enhancement of 0,0583 meters is gained.

Best case. In the best case, an enhancement of 1 meter is gained.

By estimating the average of percentage error of best cases, a value of the 21% is obtained. This is a very good result when dealing with small RMSE values. To better validate the models, different amplitude, bias, and frequenct are used while stating the reference functions.

Reference number	Reference type	EKF RMSE	DVS RMSE
1	Random wave	4,5010	4,2768
2	Random wave	4,5497	4,1002
3	Random wave	4,4776	4,4193
4	Random wave	4,5077	4,2417
5	Random wave	4,4943	4,3151
6	Random wave	4,4893	4,3449
7	Random wave	4,5869	4,1301
8	Random wave	4,5616	4,0922
9	Random wave	4,5363	4,1278
10	Random wave	4,5195	4,1860
11	Sine wave	4,4438	3,6936
12	Sine wave	4,4428	3,6958
13	Sine wave	4,4379	3,6893
14	Sine wave	4,3883	3,9043
15	Sine wave	4,3608	4,1795
16	Sine wave	4,3734	4,0435
17	Sine wave	4,4765	4,0274
18	Sine wave	4,4737	3,9857
19	Sine wave	4,4682	3,9097
20	Sine wave	4,7483	3,7483

Table 6.2: List of the 20 RMSE values obtained from EKF computation and DVS computation of **position y**.

Two charts are represented to better figure out the obtained RMSE values, referred to the **y position** and coming from the design of the EKF and the DVS. The orange lines are the RMSE amounts obtained from the EKF design, while the blue lines are the RMSE amounts coming from the DVS design. The overall RMSE measurements coming from the DVS design are lower (and so, better) than the ones coming from the EKF design.

Figure 6.4: Histogram of RMSE values referred to the **y position**.

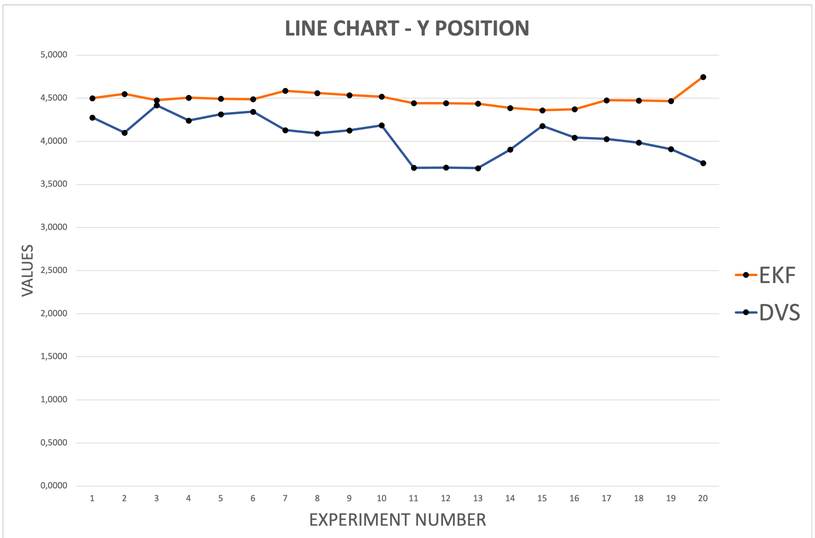

Figure 6.5: Line chart of RMSE values referred to the **y position**.

In Table 6.3, the obtained performances by stating the $\mathbf{v}_x$ **velocity** are depicted. An overall of 20 multiple validation data sets are initialized. Some random waves and sine waves are used as reference functions in the validation data set. From the obtained values there is evidence of a small improvement while using the DVS instead of the EKF. The worst and the best case are illustrated below:

Worst case. In the worst case, an enhancement of 1,1370 meters is gained.

Best case. In the best case, an enhancement of 7,2028 meters is gained.

By estimating the average of percentage error of best cases, a value of the 58% is obtained. This is an excellent result when dealing with a small RMSE values. To better validate the models, different amplitude, bias, and frequency values are used while stating the reference functions. Notice the higher improvement in random cases than sine wave cases.

Reference number	Reference type	EKF RMSE	DVS RMSE
1	Random wave	12,3614	5,2432
2	Random wave	12,4915	5,2887
3	Random wave	12,2989	5,2276
4	Random wave	12,3792	5,2484
5	Random wave	10,5755	4,6896
6	Random wave	7,8327	4,2760
7	Random wave	11,6905	5,0279
8	Random wave	10,7098	4,7839
9	Random wave	12,4555	5,2744
10	Random wave	12,4106	5,2584
11	Sine wave	5,5817	3,6738
12	Sine wave	5,5816	3,6738
13	Sine wave	6,5112	3,6686
14	Sine wave	4,9980	3,8610
15	Sine wave	5,5764	3,6706
16	Sine wave	5,5825	3,6736
17	Sine wave	5,5955	3,6702
18	Sine wave	5,6399	3,6672
19	Sine wave	5,6287	3,6674
20	Sine wave	5,6170	3,6702

Table 6.3: List of the 20 RMSE values obtained from EKF computation and DVS computation of **velocity** $\mathbf{v}_x$.

Two charts are represented to better figure out the obtained RMSE values, referred to the $\mathbf{v}_x$ **velocity** and coming from the design of the EKF and the DVS. The orange lines are the RMSE amounts obtained from the EKF design, while the blue lines are the RMSE amounts coming from the DVS design. The overall RMSE measurements coming from the DVS design are lower (and so, better) than the ones coming from the EKF design.

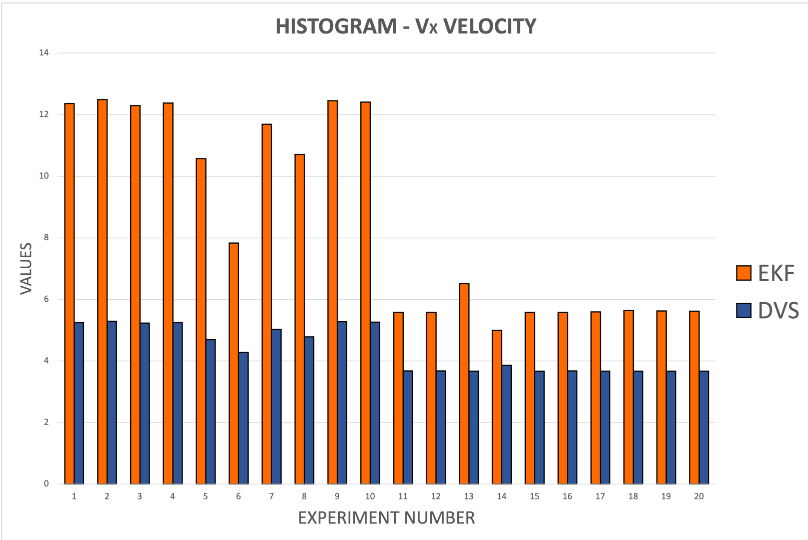

Figure 6.6: Histogram of RMSE values referred to the $\mathbf{v}_x$ **velocity**.

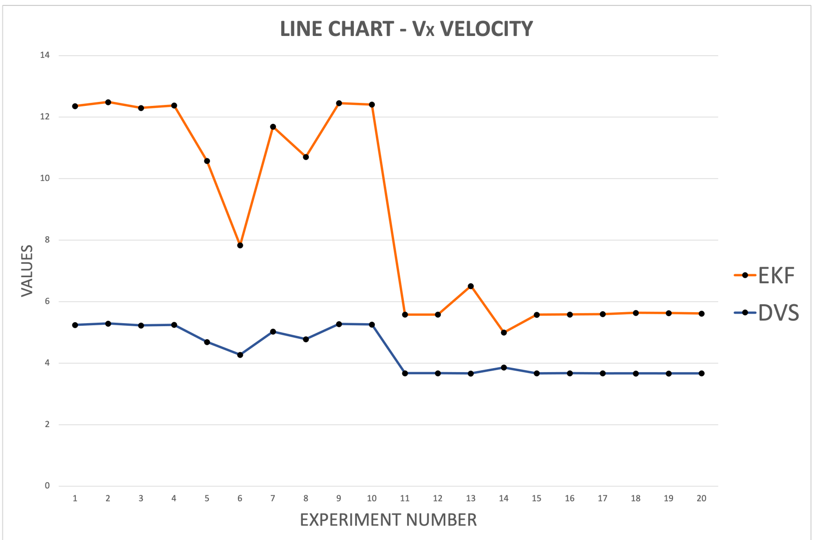

Figure 6.7: Line chart of RMSE values referred to the $\mathbf{v}_x$ **velocity**.

In Table 6.4, the obtained performances by stating the $\mathbf{v}_y$ **velocity** are depicted. An overall of 20 multiple validation data sets are initialized. Some random waves and sine waves are used as reference functions in the validation data set. From the obtained values there is evidence of a small improvement while using the DVS instead of the EKF. The worst and the best case are illustrated below:

Worst case. In the worst case, an enhancement of 0,0848 meters is gained.

Best case. In the best case, an enhancement of 6,7353 meters is gained.

By estimating the average of percentage errors of best cases, an improvement of the 65% is obtained. This is an excellent result when dealing with relative small RMSE values. To better validate the models, different amplitude, bias, and frequency values are used while stating the reference functions. Notice the higher improvement in random cases than sine wave cases.

Reference number	Reference type	EKF RMSE	DVS RMSE
1	Random wave	10,3585	3,6400
2	Random wave	10,4646	3,7293
3	Random wave	10,3076	3,6019
4	Random wave	10,3731	3,6516
5	Random wave	9,0266	3,8347
6	Random wave	6,9565	4,5919
7	Random wave	9,8751	3,7775
8	Random wave	9,1325	3,9237
9	Random wave	10,4352	3,7034
10	Random wave	10,3986	3,6724
11	Sine wave	4,5617	2,2734
12	Sine wave	4,5616	2,7432
13	Sine wave	4,3885	4,3037
14	Sine wave	4,6749	3,0509
15	Sine wave	4,5629	2,7490
16	Sine wave	4,5610	2,7440
17	Sine wave	4,5613	2,7545
18	Sine wave	4,5524	2,7780
19	Sine wave	4,5525	2,7769
20	Sine wave	4,5551	2,7642

Table 6.4: List of the 20 RMSE values obtained from EKF computation and DVS computation of **velocity** $\mathbf{v}_y$.

Two charts are represented to better figure out the obtained RMSE values, referred to the $\mathbf{v}_y$ **velocity** and coming from the design of the EKF and the DVS. The orange lines are the RMSE amounts obtained from the EKF design, while the blue lines are the RMSE amounts coming from the DVS design. The overall RMSE measurements coming from the DVS design are lower (and so, better) than the ones coming from the EKF design.

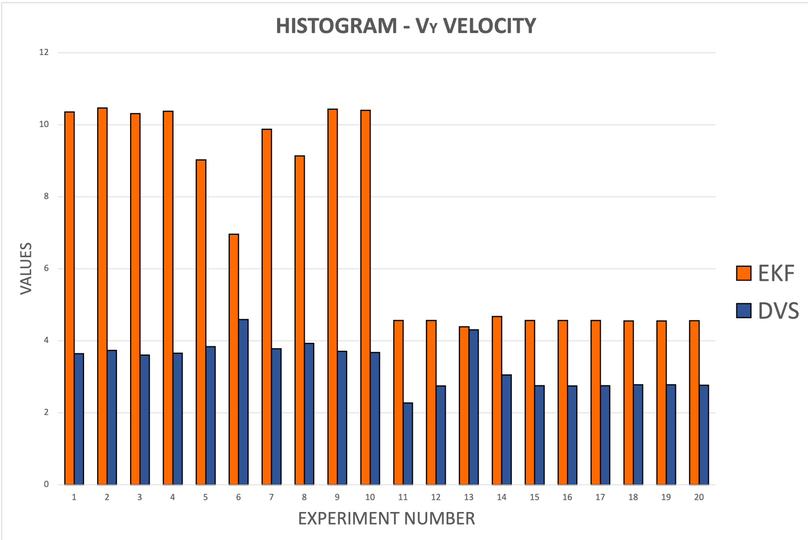

Figure 6.8: Histogram of RMSE values referred to the $\mathbf{v}_y$ **velocity**.

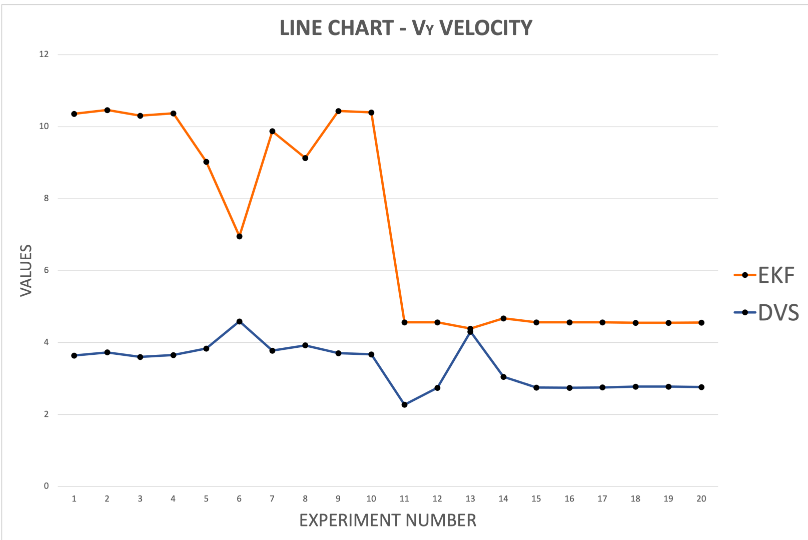

Figure 6.9: Line chart of RMSE values referred to the $\mathbf{v}_y$ **velocity**.

Chapter 7

Conclusions

The aim of this thesis is to design a state observer/filter which is able to track a target using radar measurement. Some simulated data sets are used. A two-step procedure is usually pursued by identifying a system model from an experimental data set, and then by designing the filter (EKF) based on the identified model. To better deal with nonlinearities in the system, an alternative option is the so-called one-step procedure. This approach involves the direct design of the filter (DVS) from the data set. The Extended Kalman Filter is schemed using a proper Simulink block, while the Direct Virtual Sensor is planned by using the System Identification Toolbox. Both the obtained models have been validated using Simulink. The obtained performances, in terms of root-mean-square estimation error from the two filters, are compared. The results from the simulations show better performances of the DVS than the ones of the EKF. Considering the motivations described above, the proposed process (one-step procedure) is the best choice.

Bibliography

[1] Wing Ip Tam. «Tracking filters for radar systems». PhD thesis. 1999 (cit. on pp. 2, 34).

[2] Merrill I Skolnik. «Introduction to radar». In: *Radar handbook* 2 (1962), p. 21 (cit. on pp. 2, 19).

[3] «Converted state equation Kalman filter for nonlinear maneuvering target tracking». In: *Signal Processing* 202 (2023), p. 108741. ISSN: 0165-1684. DOI: `https://doi.org/10.1016/j.sigpro.2022.108741` (cit. on p. 2).

[4] Steven Zollo and Branko Ristic. «On polar and versus Cartesian coordinates for target tracking». In: *ISSPA'99. Proceedings of the Fifth International Symposium on Signal Processing and its Applications (IEEE Cat. No. 99EX359).* Vol. 2. IEEE. 1999, pp. 499–502 (cit. on p. 2).

[5] Inam Ullah, Xin Su, Jinxiu Zhu, Xuewu Zhang, Dongmin Choi, and Zhenguo Hou. «Evaluation of localization by extended Kalman filter, unscented Kalman filter, and particle filter-based techniques». In: *Wireless Communications and Mobile Computing* 2020 (2020), pp. 1–15 (cit. on p. 2).

[6] Carlo Novara, Fredy Ruiz, and Mario Milanese. «Direct filtering: A new approach to optimal filter design for nonlinear systems». In: *IEEE Transactions on Automatic Control* 58.1 (2012), pp. 86–99 (cit. on pp. 2, 3).

[7] Lianmeng Jiao, Quan Pan, Yan Liang, and Feng Yang. «A nonlinear tracking algorithm with range-rate measurements based on unbiased measurement conversion». In: *2012 15th International Conference on Information Fusion.* IEEE. 2012, pp. 1400–1405 (cit. on p. 2).

[8] Caglar Yardim, Peter Gerstoft, and William S Hodgkiss. «Tracking refractivity from clutter using Kalman and particle filters». In: *IEEE Transactions on Antennas and Propagation* 56.4 (2008), pp. 1058–1070 (cit. on p. 2).

[9] Mario Milanese, Carlo Novara, Kenneth Hsu, and Kameshwar Poolla. «The filter design from data (FD2) problem: Nonlinear Set Membership approach». In: *Automatica* 45.10 (2009), pp. 2350–2357. ISSN: 0005-1098. DOI: `https://doi.org/10.1016/j.automatica.2009.06.014` (cit. on pp. 3, 7, 9).

[10] M Milanese, C Novara, K Hsu, and K Poolla. «Nonlinear virtual sensors design from data». In: *IFAC Proceedings Volumes* 39.1 (2006), pp. 576–581 (cit. on p. 3).

[11] Qiang Li, Ranyang Li, Kaifan Ji, and Wei Dai. «Kalman filter and its application». In: *2015 8th International Conference on Intelligent Networks and Intelligent Systems (ICINIS)*. IEEE. 2015, pp. 74–77 (cit. on p. 4).

[12] Carlo Novara. «Nonlinear Control and Aerospace applications: lecture notes». In: *Politecnico di Torino* (2020) (cit. on p. 4).

[13] Mark A Richards, Jim Scheer, William A Holm, and William L Melvin. *Principles of modern radar*. Vol. 1. Citeseer, 2010 (cit. on pp. 11–19, 22, 23, 25, 28).

[14] Martin Schneider. «Automotive radar-status and trends». In: *German microwave conference*. Citeseer. 2005, pp. 144–147 (cit. on p. 25).

[15] Liu Zhaohua and Gao Bochao. «Radar sensors in automatic driving cars». In: *2020 5th International Conference on Electromechanical Control Technology and Transportation (ICECTT)*. IEEE. 2020, pp. 239–242 (cit. on p. 25).

[16] X Rong Li and Vesselin P Jilkov. «Survey of maneuvering target tracking. Part I. Dynamic models». In: *IEEE Transactions on aerospace and electronic systems* 39.4 (2003), pp. 1333–1364 (cit. on p. 33).

[17] The MathWorks Inc. *System Identification toolbox*. Natick, Massachusetts, United States. URL: `https://it.mathworks.com/help/ident/index.html?s_tid=CRUX_lftnav` (cit. on p. 40).

[18] Ljung Lennart. *System Identification: Theory for the User*. Prentice Hall PTR, 1999. ISBN: 0136566952 (cit. on p. 40).